TÜBİTAK

Turkish Journal of Earth Sciences

http://journals.tubitak.gov.tr/earth/

Research Article

Turkish J Earth Sci
(2014) 23: 386-411

doi:10.3906/yer-1307-17

Geology, mineralogy, geochemistry, and depositional environment of a Late Miocene/Pliocene fluviolacustrine succession, Cappadocian Volcanic Province, central Anatolia, Turkey

Ersel GÖZ[1], Selahattin KADİR[1,*], Ali GÜREL[2], Muhsin EREN[3]

[1]Department of Geological Engineering, Eskişehir Osmangazi University, Eskişehir, Turkey
[2]Department of Geological Engineering, Niğde University, Niğde, Turkey
[3]Department of Geological Engineering, Mersin University, Mersin, Turkey

Received: 23.07.2013 • **Accepted:** 14.05.2014 • **Published Online:** 17.06.2014 • **Printed:** 16.07.2014

Abstract: This paper investigates the mineralogy, geochemistry, and depositional environment of Late Miocene/Pliocene fluviolacustrine deposits, including multiple ignimbrite levels and andesitic and basaltic lavas, within the Cappadocian Volcanic Province (CVP) of central Anatolia, Turkey. Palaeosols and calcretes formed within these terrestrial sedimentary rocks under near-surface or surface conditions. The palaeosols are composed predominantly of smectite ± illite with feldspar, quartz, calcite, opal-CT, and amphibole, and the calcretes mainly of calcite with minor feldspar, quartz, and accessory smectite ± palygorskite. The palygorskite occurs on and between the calcite crystals in the calcretes and at the edges of smectite flakes within the palaeosols, indicating an in situ formation from evaporated alkaline water rich in Si and Mg and poor in Al under arid or seasonally arid climatic conditions. In the palaeosols and calcretes, negative Ba, Nb, Ce, Sr, and Ti anomalies and an enrichment of light rare earth elements relative to medium rare earth elements and heavy rare earth elements, with a distinct negative Eu anomaly, likely reflect the alteration of feldspars and amphiboles in the ignimbrite. The alteration of the ignimbrites caused the depletion of SiO_2, Al_2O_3+Fe_2O_3, TiO_2, and K_2O through the precipitation of smectite ± illite in the palaeosols and CaO in the form of calcite in the calcretes. The $\delta^{18}O$ values of the calcretes and limestones range from –8.71‰ to –10.71‰, which are mainly related to the involvement of high-elevation meteoric water, whereas the $\delta^{13}C$ values for the same rocks vary between –1.97‰ and 5.71‰. The positive $\delta^{13}C$ values for the limestones reflect calcite precipitation in isotopic equilibrium with meteoric water in a lake. The slightly negative $\delta^{13}C$ values of the lacustrine limestone carbonates may indicate precipitation from a relatively thick water column and an inflow of surface or groundwater through the ignimbrites with high Ba/Sr values. Conversely, the calcrete $\delta^{13}C$ values (3.0‰ to 4.97‰) may suggest a pedogenic origin with low plant respiration rates and a predominance of C_4 plants. Based on stable oxygen isotope values from the lake sediments and calcretes, this study suggests that the global warming trend that followed the Late Miocene continued into the Pliocene within the CVP.

Key words: Cappadocian Volcanic Province, fluviolacustrine sediments, palaeosol, calcrete, stable isotopes

1. Introduction

Investigation of lakes in the geological record, particularly in the field of limnogeology, has progressed rapidly over the past 2 decades (Gierlowski-Kordesch and Rust, 1994; Last, 1994; Valero Garcés et al., 1997; Bohacs et al., 2000, 2003). Consistent with this worldwide pattern, the mineralogy, petrography, and geochemistry of volcanic and pyroclastic rocks (especially ignimbrites) and the tectonics of the Cappadocian Volcanic Province (CVP) have been studied by many researchers (Beekman, 1966; Pasquaré, 1968; Innocenti et al., 1975; Pasquaré et al., 1988; Temel, 1992; Göncüoğlu and Toprak, 1992; Le Pennec et al., 1994, 2005; Schumacher and Mues-Schumacher, 1996; Toprak, 1996, 1998; Schumacher and Schumacher, 1997; Temel et al., 1998; Dirik, 2001; Viereck-Goette et al., 2010). In this region, the volcano-sedimentary rocks and associated palaeosols and calcretes have received little attention (Le Pennec et al., 2005; Gürel and Kadir, 2006, 2008, 2010; Gürel and Yıldız, 2007; Gürel, 2009; Yavuz-Işık and Toprak, 2010; Kadir et al., 2013). Additionally, no information has been provided concerning the local palaeoclimates, and the effects of the Messinian Salinity Crisis on terrestrial areas surrounding the Mediterranean Sea are currently a matter of discussion. Therefore, the goals of this paper are to describe the mineralogy, geochemistry, and depositional environment of the Late Miocene/Pliocene fluviolacustrine deposits and associated palaeosols and calcretes within the CVP and to interpret the palaeoenvironmental and palaeoclimatic evolution data.

* Correspondence: skadir_esogu@yahoo.com

2. Geological setting

The study area is located within the CVP, a high plateau situated approximately 1400–1500 m above mean sea level (Aydar et al., 2012). The plateau extends 300 km NE–SW and is 60 km wide. During the Middle to Late Miocene, the entire area emerged and became the site of erosion, forming a large plateau, due to the collision of the Afro-Arabian plate with the Eurasian plate. Subsequently, the region has experienced complex Neotectonic deformation since the Late Miocene/Pliocene. Many faults and intracontinental basins in this region were either formed or reactivated during this period, and the region is associated with intense volcanism (Dirik, 2001). In the northern part of the CVP, a tectonic depression was filled by lacustrine and fluvial deposits, including volcanic intercalations from the Late Miocene to Late Quaternary, based on palaeontological, palynological, and radiometric data. These deposits are the sediments of the Ürgüp Basin and have been previously named the Ürgüp Formation (Pasquaré, 1968; Viereck-Goette et al., 2010). This stratigraphic interval also represents the Late Miocene phase of the Messinian Salinity Crisis.

The CVP mainly comprises ignimbrites at different stratigraphic levels, as well as andesitic and basaltic lavas. These volcanic rocks are intercalated with Late Miocene/Pliocene fluviolacustrine deposits (Table 1). In the province, the volcano-sedimentary units discordantly overlie the basement rock, including the Niğde Massif to the south and the Kırşehir Massif to the north (Figure 1). The basement rocks consist of Palaeozoic-Cretaceous metamorphic (schist, marble, and metagabbro) and Upper Cretaceous ophiolitic rocks (Schumacher et al., 1990; Toprak, 1996). In the region, Pasquaré (1968) classified the volcaniclastic, siliciclastic, and carbonate sedimentary rocks, as well as the basaltic flows of the Ürgüp Basin, as members of the Ürgüp Formation. These are the Kavak, Zelve, Sarımaden Tepe (or Sofular of Viereck-Goette et al., 2010; Figure 2), Cemilköy, Tahar, Gördeles, Kızılkaya, and İncesu ignimbrites; the Topuzdağ and Çataltepe basalts; and the Bayramhacılı and Kışladağ members. The Bayramhacılı member includes fluviolacustrine sedimentary rocks, such as conglomerates, sandstones, limestones, marlstones, and diatomites, whereas the Kışladağ member comprises lacustrine limestones and diatomites. The Kışladağ member contains ostracod and gastropod fossils within the lacustrine limestones. The Kavak, Zelve, and Sarımaden Tepe ignimbrites are mainly white to grey, and the Cemilköy ignimbrites are pale grey and nonwelded with chimney structures (Le Pennec et al., 1994). The pink Tahar ignimbrite, pale grey Gördeles ignimbrite, and red to pink Kızılkaya ignimbrite are widespread welded ignimbrites, characterised by columnar jointing (Le Pennec et al., 1994). The red to pink Incesu ignimbrite crops out outside of the study area. The Ürgüp Formation is overlain by Quaternary alluvium (Figure 1). The age of the ignimbrite succession, based on $^{40}Ar/^{39}Ar$ plagioclase and U-Pb zircon dating, is 9 to 1 Ma (Aydar et al., 2012).

3. Lithologic and pedogenic descriptions

The Bayramhacılı member comprises sedimentary rocks of fluvial and lacustrine deposits (Figures 3 and 4) and is observed in the Başköy (P1), Güzelöz (P2, P3), Şahinefendi (P4), Kışladağ (P5), Aktepe (P6), and Bayramhacılı (P7) profiles. The lithologic and pedogenic descriptions of the profiles are given as follows.

The fluvial deposits comprise massive conglomerate, trough cross-bedded sandstone, mudstone, and associated palaeosols and calcretes (Figures 2 and 5a–5e). The calcretes and palaeosols appear in the fluvial sedimentary rocks (Table 1; Figure 3). In the study area, 3 types of palaeosol are recognised (Retallack, 1990): (i) an inceptisol, (ii) a histosol, and (iii) an aridisol (for details, see Table 1). The calcretes occur in and/or on fluvial mudstones and the palaeosols (Figure 5e) in nodular, tubular, massive, and fracture infill forms.

The lacustrine units in the study area are composed of limestones, marlstones, and diatomites (Figures 2 and 5f–5h). The limestones are brecciated and contain gastropod and ostracod fossils. The marlstone occurs mainly in profile P7 and is white to grey in colour and thinly laminated. The diatomite is white in colour and exhibits massive to laminated bedding.

4. Materials and methods

In the field, stratigraphic sections were measured to study lateral and vertical lithological variations within the Bayramhacılı (Late Miocene) and Kışladağ (Early-Middle Pliocene) members of the Neogene Ürgüp Formation (Figure 3). Ninety-three characteristic samples of Late Miocene/Pliocene limestone, conglomerate, sandstone, mudstone, and marlstone were collected from the study area. Thin sections were prepared from these samples to describe their petrographic properties. The limestones and siliciclastic sedimentary rocks were described according to the Dunham (1962) and Miall (1996) classifications, respectively.

The mineralogical characteristics of the samples were determined by powder X-ray diffractometry (Rigaku Geigerflex) and scanning electron microscopy (SEM) (JEOL JSM 84A-EDX). Fine siliciclastic and carbonate samples were prepared for clay mineral analyses (size fraction <2 μm) by separating the clay fraction by sedimentation, followed by centrifugation of the suspension after an overnight dispersion in distilled water. The clay particles were dispersed by ultrasonic vibration

Table 1. Summary of the lithologic and pedogenic descriptions and the palaeoenvironmental interpretations.

Facies	Codes	Description	Interpretation
Massive conglomerate	Gm	Grain-supported conglomerate; massive, pink-coloured, unsorted, and rounded; clasts are approximately 5 cm in size; normal grading; lens-shaped layers; average thickness 0.5 to 1 m; containing clasts derived from gabbro, serpentinite, metamorphic rocks, pumice, sandstone, and mudstone; matrix consists of clay, silt, and sand; outcrops are relatively limited and horizontally extend between 3 and 5 m.	River channel fill
Trough-cross-bedded sandstone	St	Fine- to coarse-grained sands containing current ripples with curved foresets and asymptotic downlap at their bases; layer thickness varies from 15 to 20 cm, and trough-cross-bed sets have a thickness of approximately 5 mm, laterally extending 5-10 m.	River sheet-flood to main-channel deposits
Mudstone	Fm	Brown-coloured mudstone, massive; average thickness 0.5 m; lateral extent 4 km.	River floodplain deposits
--	AL-P	(1) Not well-differentiated soil profile including B and C horizons, B horizon is appreciably enriched in sand and gravel, light brown in colour, a recompaction thickness of 1–2 m; (2) a surface organic soil horizon of uncarbonaceous peat and a recompaction thickness of 30 cm; (3) soil with muddy and fine-grained, locally scattered pebbles and light pink colour, as well as rarely a very thin calcareous layer near the surface of the horizon, a recompaction thickness of 1–2 m; lateral extent 5–6 km.	Palaeosol; (1) inceptisol, (2) histosol, (3) aridisol; river floodplain deposits
--	AL-Ca	(1) Pink- or white-coloured massive carbonate level comprising lithic, tuffaceous, and pumice clasts cemented and partially replaced by calcite, grading downward into calcareous tuff and pumice clasts; thickness ranges from 50 cm to 70 cm, and characterised by nonuniform cementation, which accentuates surface cavities; (2) carbonate level, pink-coloured massive comprising sand grain pumice, rock fragment; thickness range of 1–20 cm and characterised by micritic to sparitic cementation; lateral extent 1–500 m developed in palaeosol.	Calcrete; (1) tube and massive calcrete, (2) nodular and fracture-infill calcrete
Diatomite	AL-D	White, argillaceous massive diatomite or laminated diatomite including *Aulacoseira* (*Melosira*) *islandica* (Müller, 1895); overlies brown palaeosols; average thickness 1–2 m; lateral extent 500–600 m.	Shallow-lake environment
Marlstone	M	White to grey, finely laminated; average thickness 4–5 m; lateral extent 2–7 km.	Shallow-lake environment
Limestone	L	Micritic limestones intercalate with diatomite beds; limestones are brecciated and contain abundant microscopic rhizolith holes; biogenic components are mainly freshwater mollusc fragments (gastropods) and ostracods present rarely; locally contain coaly organic matter; lateral extent 10–15 km.	Shallow-lake environment

for approximately 15 min. Three oriented specimens of the <2 μm fraction of each sample were prepared by air drying, an ethylene-glycol solvation at 60 °C for 2 h, and a thermal treatment at 550 °C for 2 h. Semiquantitative estimates of the rock-forming minerals were obtained by using the external standard method of Brindley (1980). The relative abundances of clay-mineral fractions were determined using their basal reflections and the mineral intensity factors of Moore and Reynolds (1989). Representative clay- and carbonate-dominated bulk samples were prepared for SEM analyses by mounting the fresh, broken surface of each sample onto an aluminium sample holder with double-sided tape and thinly coating them (350 Å) with gold using a Giko ion coater.

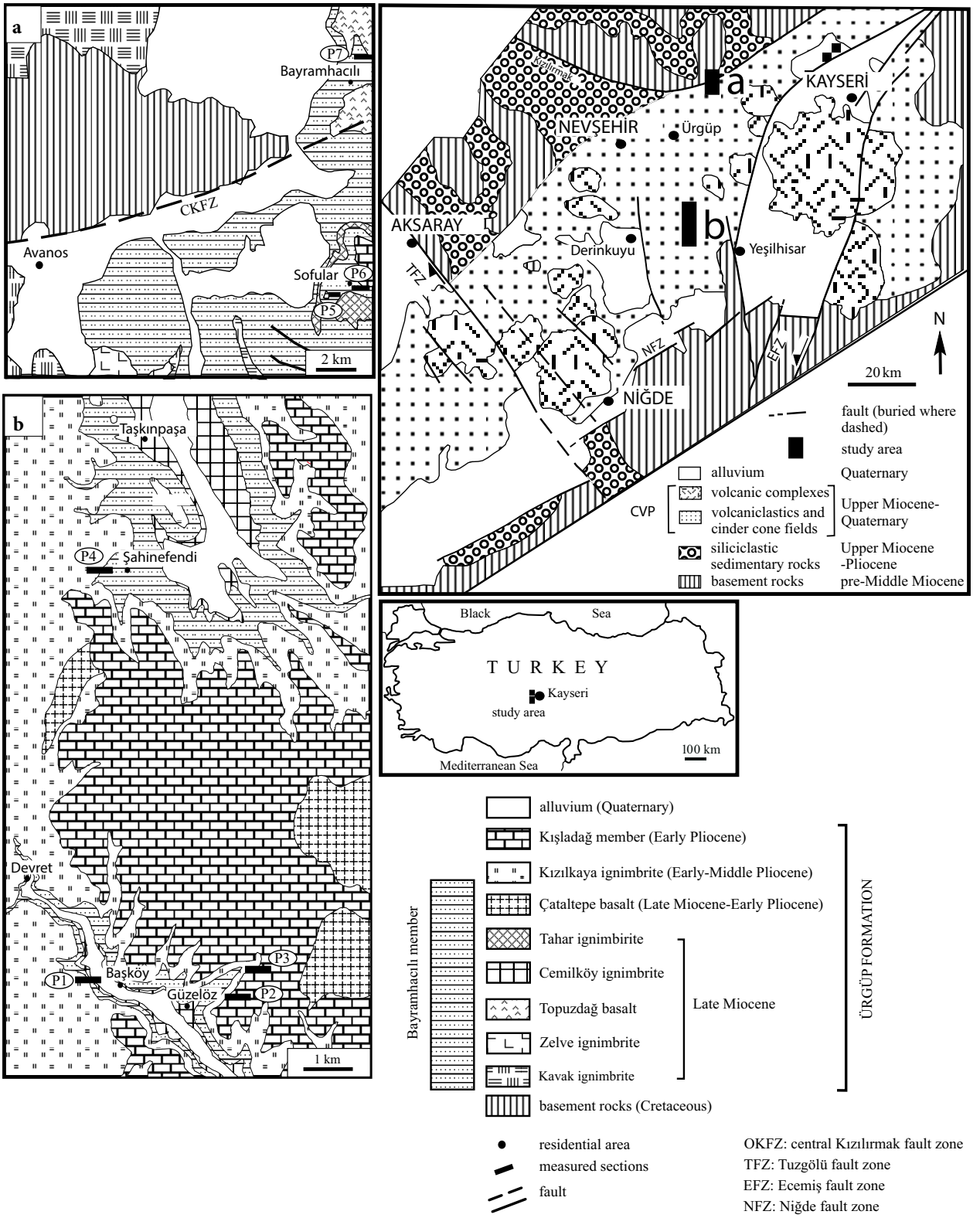

Figure 1. Simplified geological map of the study area (modified from Toprak, 1998; Gürel and Kadir, 2006; and Yavuz-Işık and Toprak, 2010).

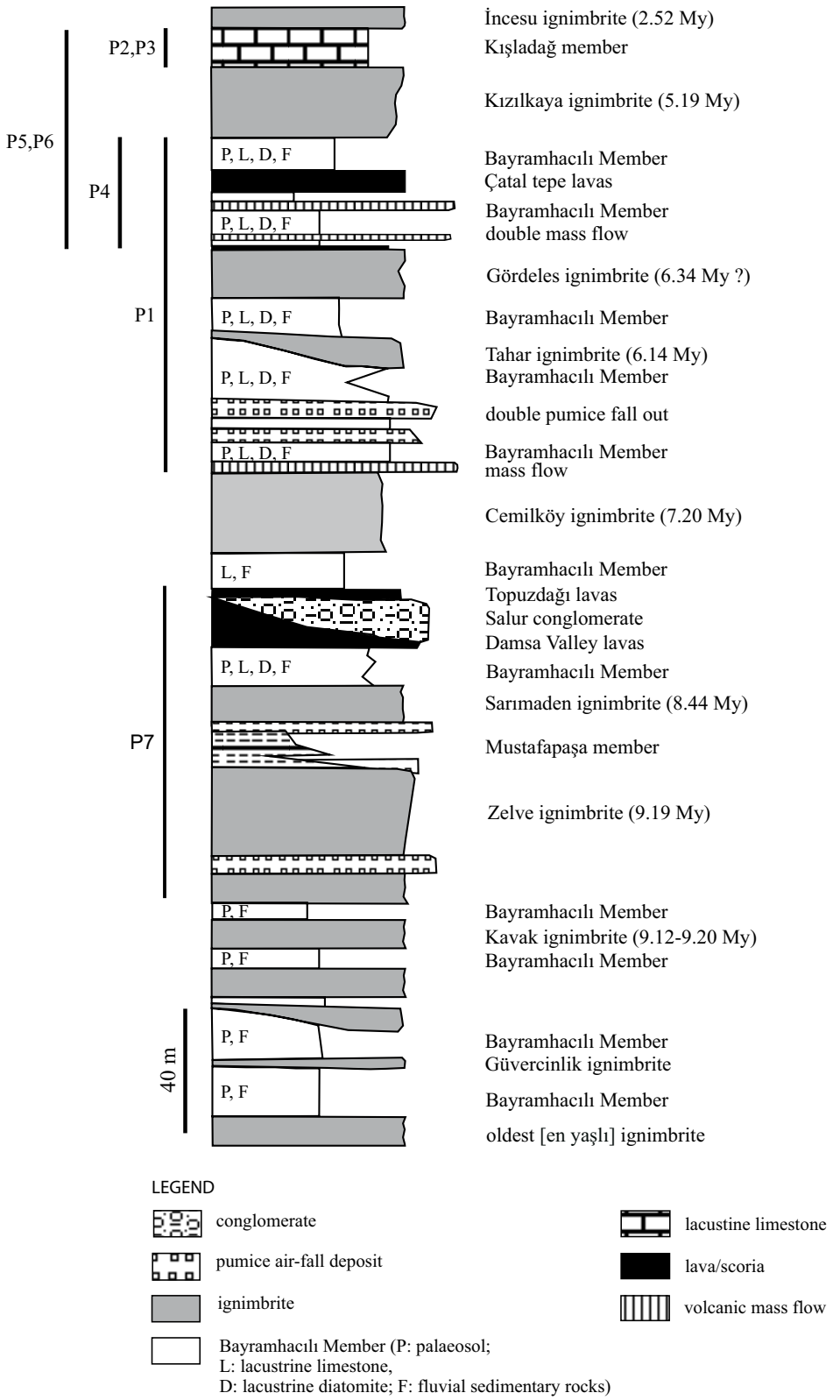

Figure 2. Generalised stratigraphic column of the study area (modified after Viereck-Goette et al., 2010).

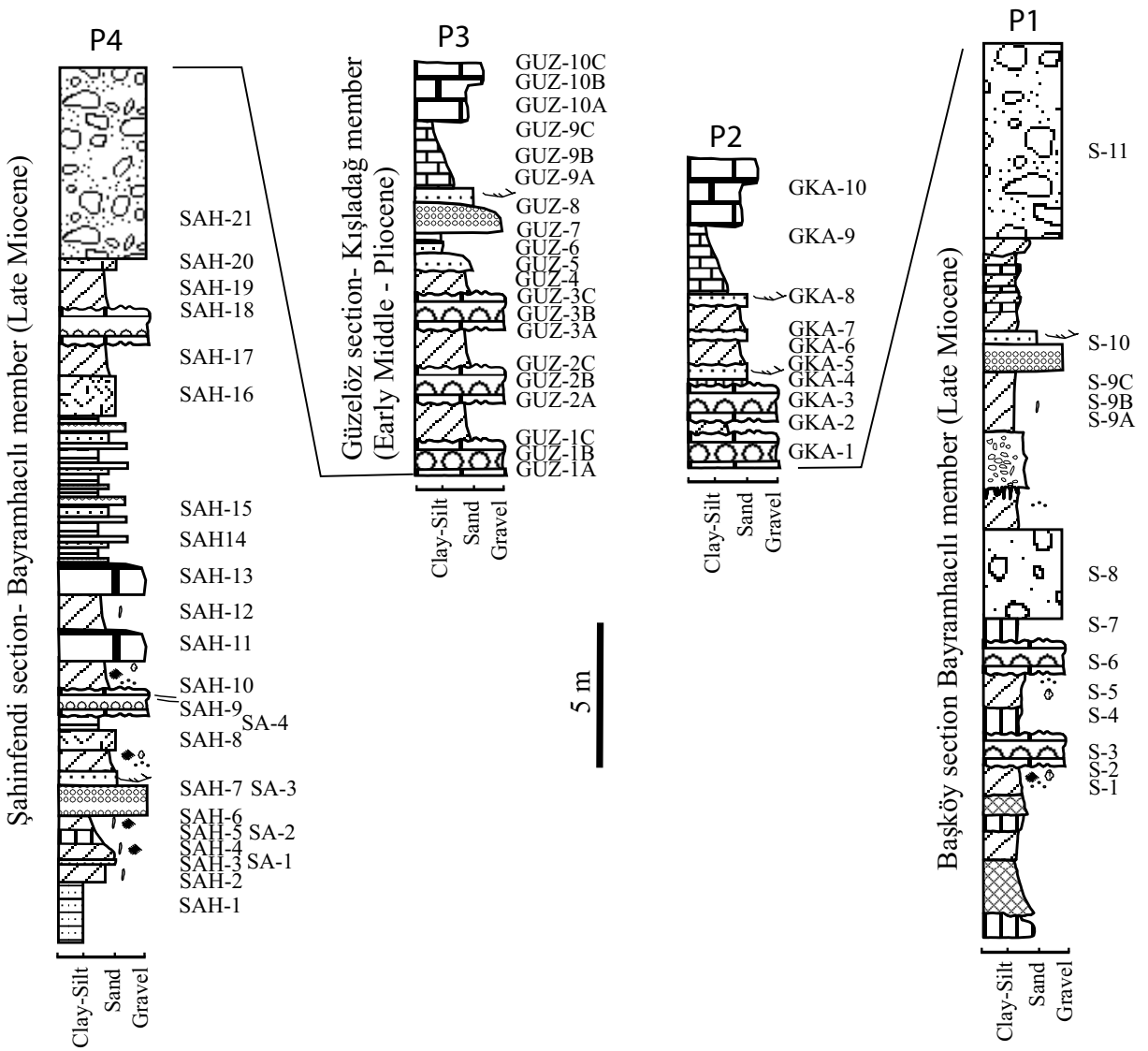

Figure 3. Correlation of measured sections within the study area. P1: Başköy section (S), P2–P3: Güzelöz section (GKA, GUZ), P4: Şahinefendi section (SAH), P5-P6: Sofular section (KIS, AK), P7: Bayramhacılı section (BH).

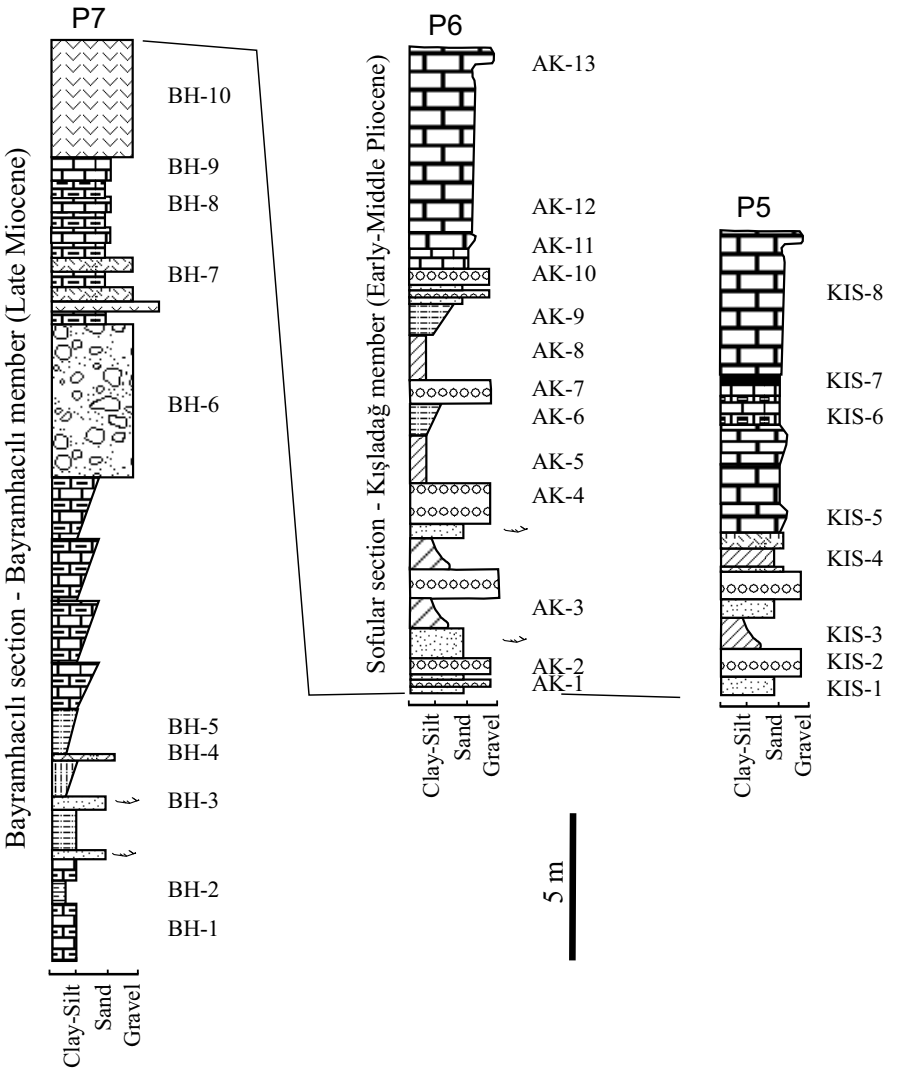

Figure 3. (continued).

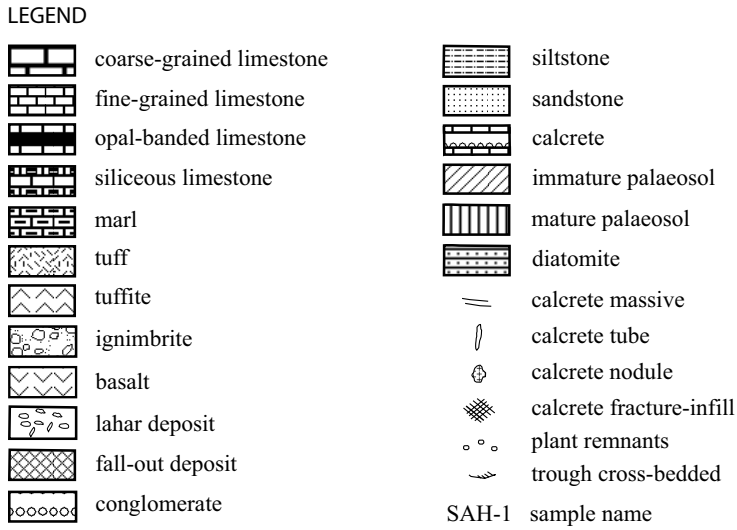

Figure 3. (continued).

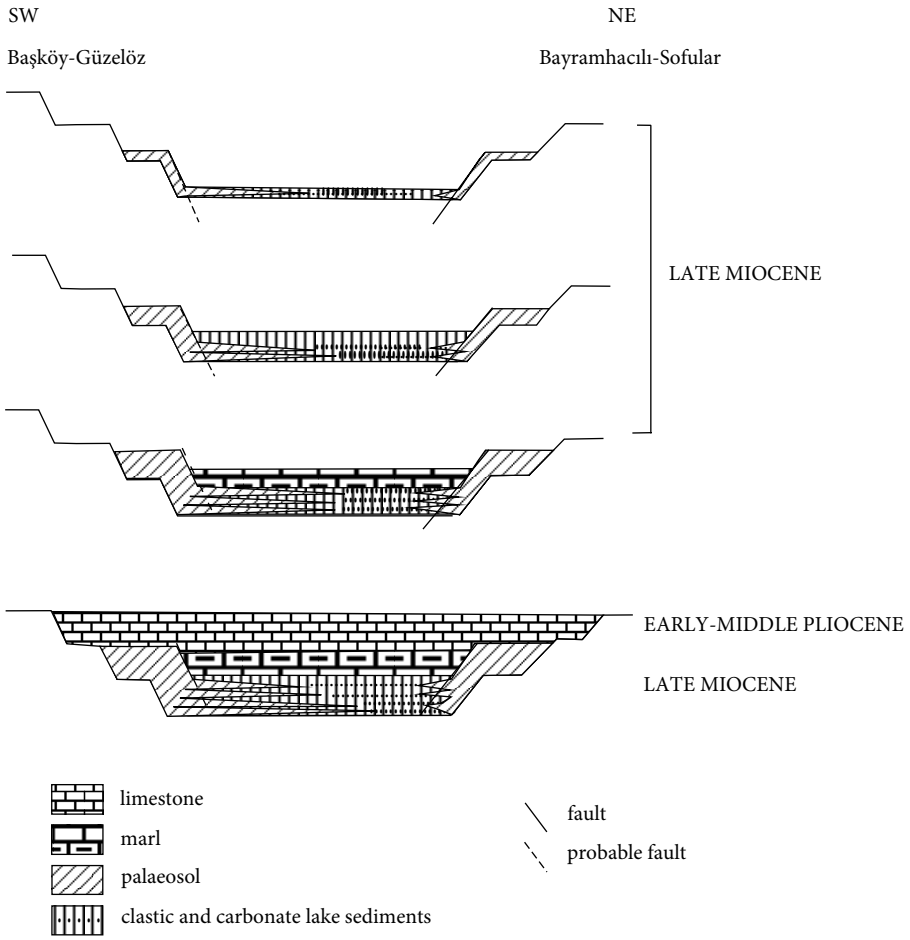

Figure 4. Depositional model showing the evolution of Late Miocene/Pliocene fluviolacustrine deposits in the study area.

The chemical analysis of 25 fresh and altered whole-rock samples were performed at Acme Analytical Laboratories Ltd. (Vancouver, Canada) using ICP-AES for major and trace elements and ICP-MS for rare earth elements (REEs). The detection limits for the analyses were between 0.01 and 0.1 wt.% for the major elements, 0.1 and 5 ppm for the trace elements, and 0.01 to 0.5 ppm for the REEs.

The stable isotope analyses ($\delta^{18}O$ and $\delta^{13}C$) were performed at the Iso-Analytical Ltd. laboratories (Crewe, UK). The samples for isotope analysis were selected by removing 0.5–3 mg of powder from micritic carbonates using a microdrill and avoiding any visible sparry calcite cement in the cracks. Ten powdered carbonate samples were weighed into Exetainers and then placed in an oven to dry prior to continuing the analysis to ensure there was no moisture in the samples and/or containers prior to sealing them and performing the acid conversion to carbon dioxide. The sample tubes and tubes containing the reference and control carbonates were then flushed with 99.995% helium. After flushing, 0.5 mL of phosphoric acid (H_3PO_4) was added to digest the carbonates (McCrea, 1950) by injecting it through the septum caps into the vials. The vials were left for 24 h at room temperature to allow the acid to react with the samples. After 24 h, the vials were heated to 60 °C for 2 h to ensure that all of the available carbonate was converted to carbon dioxide. The CO_2 gas liberated from the samples was then analysed by continuous-flow isotope-ratio mass spectrometry on a 20-20 mass spectrometer linked to an ANCA-G gas purification module (Europa Scientific, Crewe, UK). The isotope values are reported per mill (‰) relative to V-PDB and were calibrated against the reference material IA-R022 (iso-analytical working standard calcium carbonate, $\delta^{13}C_{V\text{-}PDB}$ = –28.63‰ and $\delta^{18}O_{V\text{-}PDB}$ = –22.69‰), NBS-18 (carbonatite, $\delta^{13}C_{V\text{-}PDB}$ = –5.01‰ and $\delta^{18}O_{V\text{-}PDB}$ = –23.2‰), and NBS-19 (limestone, $\delta^{13}C_{V\text{-}PDB}$ = 1.95‰ and $\delta^{18}O_{V\text{-}PDB}$ = –2.2‰), which were run as quality-control check samples during the analysis of the samples. The overall analytical error was 0.1‰ for $\delta^{13}C$ and 0.15‰ for $\delta^{18}O$.

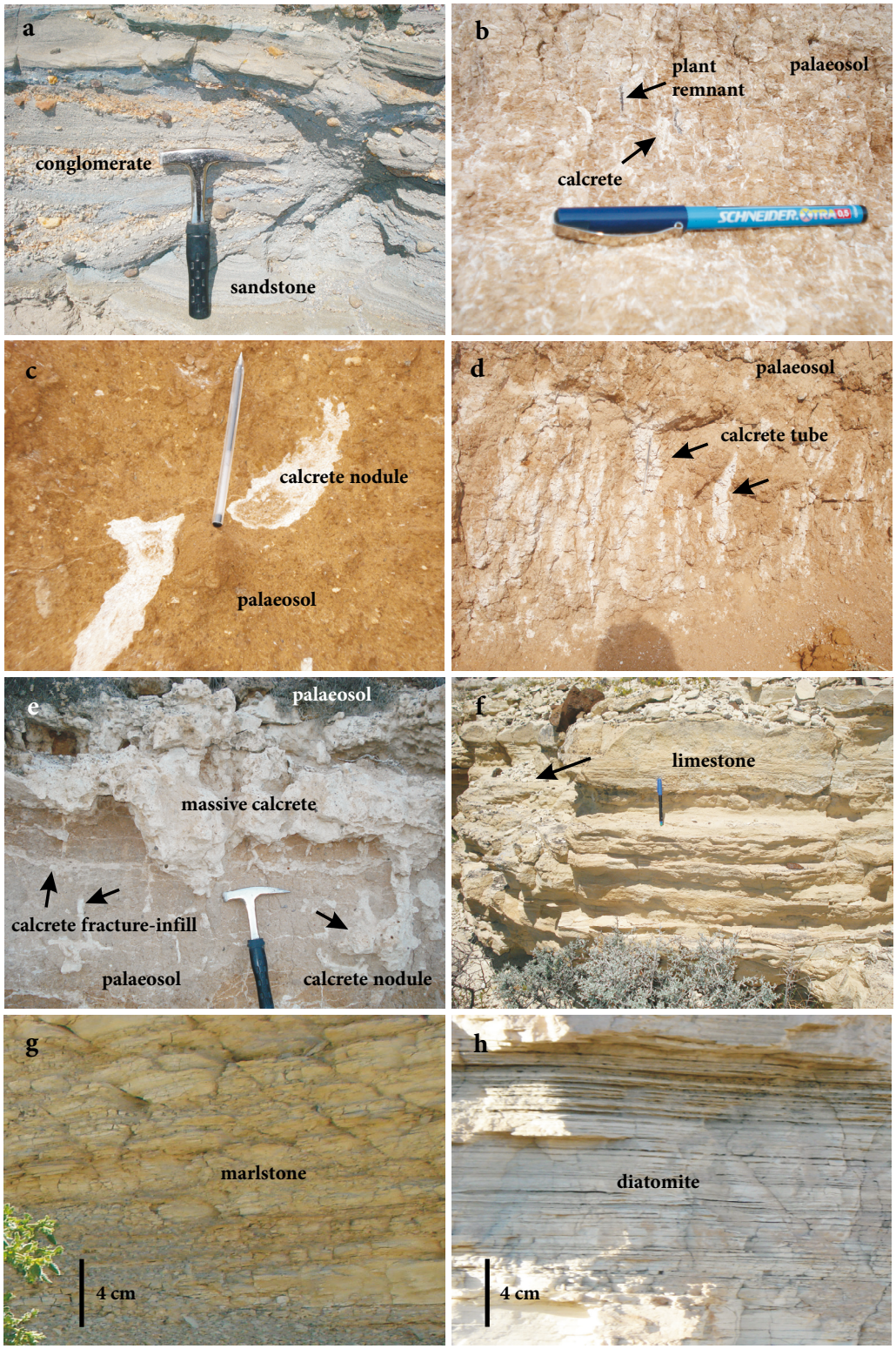

Figure 5. Field photographs of: (**a**) alternation of conglomerate and sandstone in the Bayramhacılı member in the Kışladağ section showing trough-cross-bedding (Figure 3, P5, samples AK1 and AK2; hammer length: 30 cm); **(b)** plant remains in the aridisol in the Başköy section (Figure 3, P7, sample S-7; length: 15 cm); **(c)** calcrete mottling in the moderately mature palaeosol in the Başköy section (Figure 3, P7, sample S-5); **(d)** calcrete tubes in the palaeosol in the Şahinefendi section (Figure 3, SAH-5, sample P4); **(e)** gradual transition from massive to nodular calcretes on/in the palaeosol in the Şahinefendi section (Figure 3, P4 sample SAH-9, SAH-10); **(f)** lacustrine limestone beds in the Kışladağ member, exhibiting local brecciation (arrow) (Figure 3, P5, sample KIS-7); **(g)** thinly laminated marlstone in the Bayramhacılı section (Figure 3, P7, sample DH-1); **(h)** massive and laminated diatomite in the Şahinefendi section (Figure 3, P4, SAH-1).

5. Results

5.1. Petrographic and mineralogical determinations

Certain calcrete samples developed in altered tuffs with calcitised grains, volcanic glass, amphiboles, feldspars, and opaque minerals (Figures 6a–6c). The limestone samples were classified as mudstones and wackestones (Dunham, 1962) and contain ostracod and gastropod fossils, organic material (Figures 6d and 6e), and plagioclase and volcanic glass shards.

Nontectonic cracks, possibly caused by compaction, were visible in some limestone thin sections, and these were filled with sparitic dogtooth-rim and sparitic calcite cements (Figure 6f; Atabey et al., 1998; Karakaş and Kadir, 1998; Gürel and Kadir, 2006).

The mineralogical compositions of the sedimentary rock samples collected from the study area were determined by X-ray diffractometry (Table 2). The minerals feldspar, quartz, calcite, opal-C,T and amphibole with smectite, illite, and accessory palygorskite were identified.

The calcretes consist predominantly of calcite with minor feldspar and quartz ± accessory smectite ± palygorskite, and the palaeosols are predominantly

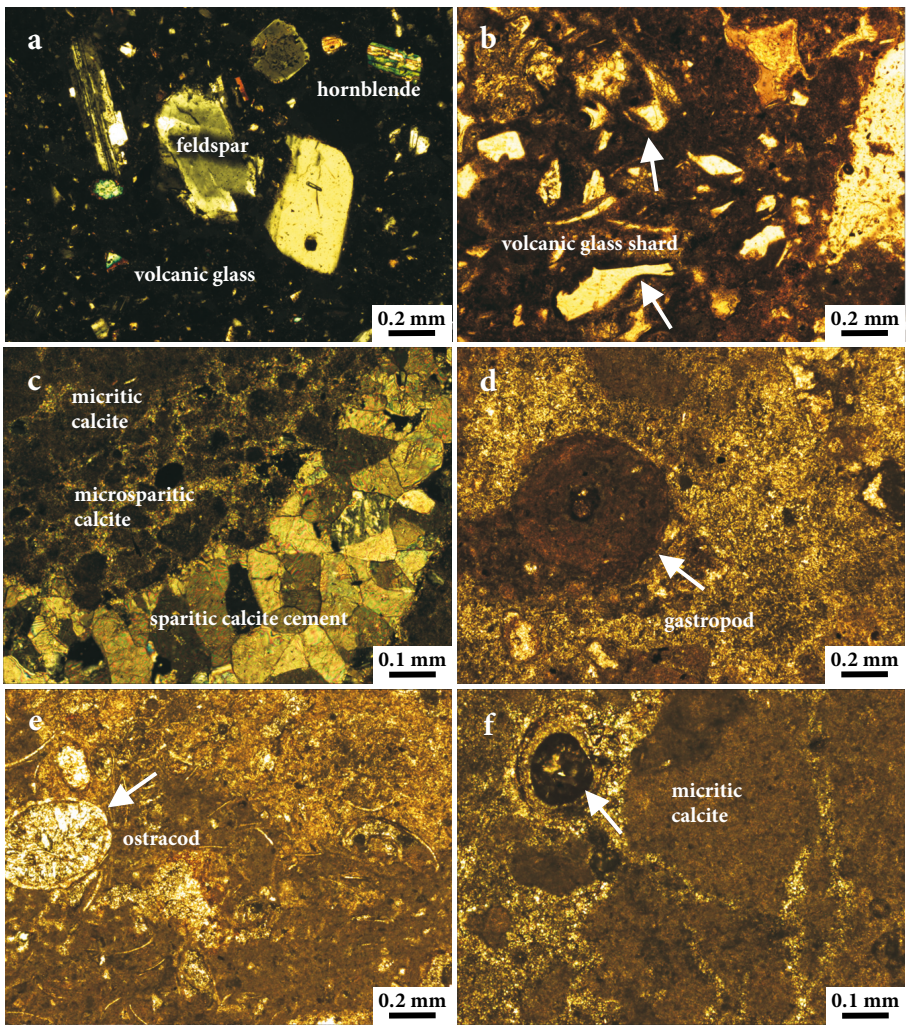

Figure 6. Photomicrographs of the following: **(a)** altered feldspar and hornblende phenocrysts in the volcanic glass groundmass of an ignimbrite (Figure 3, P1, S8, crossed polars); **(b)** devitrification of volcanic glass shards in calcrete from the Kışladağ member in the Güzelöz section (Figure 3, P2, GKA-3, plane-polarised light); **(c)** view of sparitic calcite cement in a crack of calcrete from the Kışladağ member in the Güzelöz section (Figure 3, P2, GKA-9, crossed polars); **(d)** well-preserved gastropod(?)-fossil-bearing limestone from the uppermost portion of the Kışladağ member in the Güzelöz section (Figure 3, P3, GUZ-10C, plane-polarised light); **(e)** thin curved shells of ostracods in limestone (Dunham, 1962): a wackestone, likely indicating a low-energy lacustrine environment (Figure 3, P6, AK-12, plane-polarised light); **(f)** microbrecciation developed due to the cracking of micritic limestone of the upper level of the Kışladağ member in the Sofular section. Organic material is represented by root traces. The crack is filled by microsparitic calcite cement (Figure 3, P6, AK-11, plane-polarised light).

Table 2. Mineralogical variations in the stratigraphic sections of the study area.

Sample	Rock Type	cal	qtz	op	smc	ilt/mc	pal	fds	am
SAH-13	Limestone	+++	+					acc	
GKA-10	Limestone	++++	acc						
GUZ-9A	Limestone	++++	+	+				acc	
GUZ-10A	Limestone	+++++	acc						
AK-11	Limestone	+++++			+				
KIS-7	Limestone	++++			acc				
KIS-8	Limestone	+++++							
BH-1	Marlstone	+++	+	acc	acc			acc	
S-3	Calcrete	++	acc					++	
SAH-9	Calcrete	+++	+	acc				+	acc
SAH-10	Calcrete	++++	acc					acc	
SAH-18	Calcrete	+++						+	
GKA-3	Calcrete	++	+	acc				+	
GUZ-1A	Calcrete	+++	+	acc				+	
GUZ-2A	Calcrete	++	+	+	+			++	
GUZ-2C	Calcrete	++	+	acc	+	acc		++	
GUZ-3A	Calcrete	++	acc	acc	+	acc	acc	++	
GUZ-3B	Calcrete	++	+	+				++	
GUZ-3C	Calcrete	+++	+					+	
S-1	Palaeosol	+	+	+	+			++	
S-2	Palaeosol	+	+	+	+		acc	++	
S-4	Palaeosol	acc	++	+	++				+
S-5	Palaeosol	++	acc	+	+			+	
S-7	Palaeosol		+	++	++			++	
S-9A	Palaeosol		++	+	+			+++	
S-9B	Palaeosol		+	acc				++	
S-10	Palaeosol		++					++	
SA-2	Palaeosol	+	+	+	acc				acc
SAH-2	Palaeosol	++	acc		+			++	
SAH-5	Palaeosol		+	+	acc			++	acc
SAH-12	Palaeosol	acc	+	+				++	acc
SAH-17	Palaeosol	acc	+	+	+	+		++	
SAH-19	Palaeosol	+	+	+				+	
KIS-3	Palaeosol	+	+	++	+++		acc	+++	
AK-3	Palaeosol	acc	+	++	+++	acc	acc	++++	
AK-5	Palaeosol	acc	+	+	++	acc		+++++	
GKA-2	Palaeosol	+	+	acc				++	
GKA-6	Palaeosol	+	+	+		+		++	
SAH-1	Diatomite		+++	++	++	acc		+	
GUZ-7	Diatomite		+++	++	+	+		+	
SA-3	Fluvial sedimentary rocks	++++	+					+	
SA-4	Fluvial sedimentary rocks	acc	+	+	++		acc	++	

Table 2. (continued).

SAH-3	Fluvial sedimentary rocks	+		acc				++	
SAH-14	Fluvial sedimentary rocks	++	+					+	
GKA-4	Fluvial sedimentary rocks	+	+	acc	+	+		+	
GKA-8	Fluvial sedimentary rocks	+	+	+				++	
GUZ-5	Fluvial sedimentary rocks	+	+	+	+			+++	+
BH-2	Fluvial sedimentary rocks	+++	++	acc	++++	+	acc	++	
SAH-8	Pyroclast	++		+		acc		+	

cal: calcite, qtz: quartz, op: opal-CT, smc: smectite, ilt/mc: illite/mica, pal: palygorskite, fds: feldspar, am: amphibole. +: relative abundance of mineral phase, acc: accessory, GUZ-GKA: Güzelöz, SA-SAH: Şahinfendi, S: Başköy, BH: Bayramhacılı, AK: Aktepe, KIS: Kışladağ.

smectite ± illite with feldspar, quartz, calcite, opal-CT, and amphibole. The smectite in mudstones is associated mainly with palygorskite. Feldspar and quartz are dominant in most samples, whereas calcite is abundant in the limestone and calcrete units. The limestone and marlstone units are composed mainly of calcite associated with accessory feldspar, quartz, clay minerals, and opal-CT.

Smectite is characterised by very sharp basal reflections between 14 and 15 Å. These peaks expanded to 17–18 Å following the ethylene-glycol treatment, and then collapsed to 10 Å after being heated to 550 °C. Palygorskite has a sharp diagnostic basal reflection at 10.5 Å, which was unaffected by the ethylene-glycol treatment but collapsed after being heated to 550 °C. Illite is indicated by reflections at 10 and 5 Å, and amphibole by a reflection at 8.3 Å.

5.2. Scanning electron microscopy

The SEM images indicate that popcorn- or honeycomb-form smectite occurs in the palaeosols and is generally developed on devitrified volcanic glass, having grown as bridges and fills between voids and grains (Figure 7a). Clay and carbonate minerals are present with bar-shaped structures resembling organic material (Figure 7b). Microsparitic to sparitic calcite cement is present in fine-grained limestone sample and dogtooth-type sparitic calcite crystals in cracks (Figure 7c).

The calcrete and limestone samples from the Güzelöz section contain abundant euhedral to subhedral, authigenic, rhombic calcite crystals, which were altered and dissolved. Palygorskite occurs as fibre masses and interwoven fibres grown on calcite crystals and as long fibre bundles developed authigenically at the edges of smectite flakes (Figure 7d).

5.3. Chemical analyses

The chemical analyses of the representative samples of the limestones, calcretes, palaeosols, fluvial sedimentary rocks, diatomites, gabbros, pyroclasts, and ignimbrites are provided in Table 3. The limestone and calcrete samples are characterised by the values of CaO (48.5% and 26.5%, respectively), loss on ignition (LOI) (39.4% and 24.4%), SiO_2 (8.7% and 32.8%), Al_2O_3 (1.4%), Fe_2O_3 (0.5%), MgO (0.7%), K_2O (0.2%), Sr (157 and 160 ppm), Ba (37.7 and 248.4 ppm), and Rb (12.3 and 56.7 ppm).

The CaO contents are attributed mainly to the presence of calcite, and its abundance is inversely related to SiO_2 and Fe_2O_3 (Figures 8a and 8b). The CaO values are positively correlated with the LOI values (Figure 8c) due to the clear dominance of $CaCO_3$ in the samples. The trend crosses the LOI axis at a point somewhat greater than zero, corroborating the already established clay and/or (plagioclase) feldspar contents. The clay content decreases with increasing CaO and decreasing Al_2O_3 (Figure 8d). The inverse relationship (the negative correlation between the concentration values) between CaO and Rb is only evident in the limestone samples, and a similar relationship for Sr is only evident in the calcretes (Figures 8e–8h). The Al_2O_3 values increase in the palaeosols (average: 14.2%), fluvial sedimentary rocks (average: 14.5%), diatomites (average: 13.7%), and calcretes (average: 9.0%) relative to limestone and calcrete, and they positively correlate with SiO_2, Fe_2O_3, MgO, Na_2O, TiO_2, and K_2O contents (Figures 8h–8m), indicating the presence of feldspar and smectite ± illite (see Table 3; Gürel and Kadir, 2006).

There is a positive relationship between K_2O and Rb+Ba (Figure 8n) in the volcanic material due to the presence of K-bearing minerals, such as illite/mica and feldspar, which is similar to the Early Miocene alluvial-fan to cyclic shallow-lacustrine depositional system of the Aktoprak Basin (central Anatolia) (Gürel and Kadir, 2010). The palaeosols, calcretes, and pyroclastic-ignimbritic material display similar primitive mantle-normalised (Taylor and McLennan, 1985) and chondrite-normalised (Boynton, 1984) spider diagrams, revealing strongly negative anomalies for Ba, Nb, Ce, Sr, and Ti (Figures 9a), and an enrichment of light rare earth elements (LREEs) relative to medium rare earth elements (MREEs) and heavy rare earth elements (HREEs), as well as negative Eu anomalies ($Eu_N/Eu^* = 0.61–0.80$) (Figure 9b; Table 3).

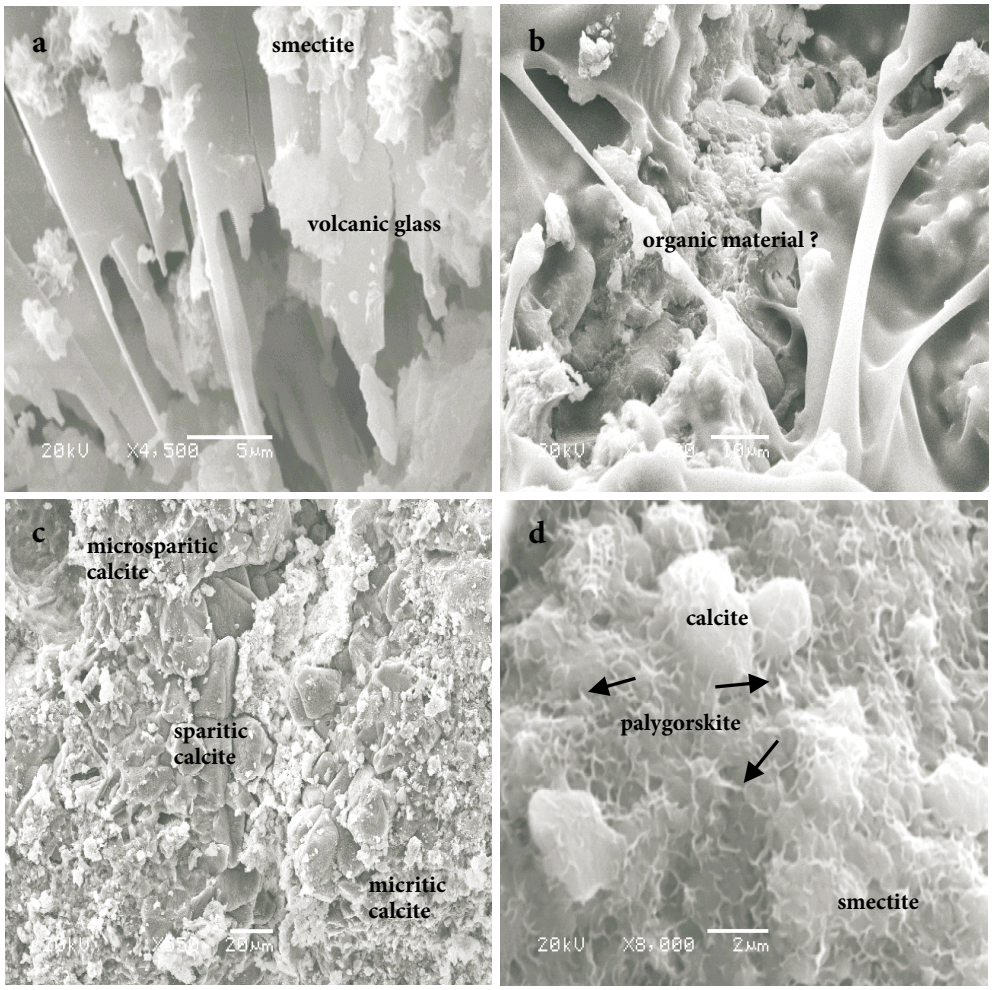

Figure 7. SEM images of the following: **(a)** smectite crystals on devitrified volcanic glass in an ignimbrite (Figure 3, P7, BH-6); **(b)** organic material (?) in the aridisol (Figure 3, P1, S-4); (**c**) euhedral, authigenic rhombic calcite, micrite, and microsparitic to sparitic calcite (dogtooth-type calcite crystal) in limestone samples (Figure 3, P2, GKA9); **(d)** development of palygorskite fibres on calcite rhombs, and palygorskite fibres edging smectite (Figure 3, P3, GUZ-3A).

The molecular alteration ratios of the limestones, calcretes, palaeosols, pyroclasts, fluvial sedimentary rocks, diatomites, and ignimbrites are provided in Table 4. These units exhibit salting, heterogenic calcification, and soil formation by hydrolysis, as well as a leaching mechanism, when compared to the normal indicator values of the Soil Survey Staff (1998) (Table 5).

5.4. Stable isotopes

The stable isotope compositions of the calcite in the limestone and calcrete samples are provided in Table 6 and Figure 10. The limestone samples yield $\delta^{18}O$ and $\delta^{13}C$ values ranging from –8.71‰ to –10.71‰ and from –1.97‰ to 5.71‰, respectively. The $\delta^{13}C$ values vary in a fairly broad range with respect to the $\delta^{18}O$ values. The $\delta^{18}O$ and $\delta^{13}C$ values of calcrete samples vary from –9.13‰ to –10.69‰ and from 4.97‰ to 3.00‰, respectively.

6. Discussion

Central Anatolia emerged during the Middle to Late Miocene and became an erosional site, eventually becoming a vast plateau (Erol, 1999). The westward escape of the Anatolian plate initiated the development of a transtensional basin in central Anatolia and imparted a NE–SW trend to the Ürgüp Basin filled by Late Miocene/Pliocene volcanic and volcano-sedimentary materials (Figure 4). The fluvial deposits accumulated in a terrestrial environment and are associated with palaeosols and calcretes. The presence of palygorskite in the calcretes is indicative of arid or seasonally arid climatic conditions (Sancho et al., 1992). Additionally, palynological analyses from the Güzelöz (Early Pliocene) and the lower part of the Bayramhacılı (Late Miocene) sections suggest steppe vegetation and arid climatic conditions (Yavuz-Işık and

Table 3. Chemical compositions of various lithofacies of the study area. ΣREE = the sum of (La-Lu)+Y; ΣLREE = the sum of La-Nd; ΣMREE = the sum of (Sm-Ho); ΣHREE = the sum of (Er-Lu); Eu/Eu*=Eu/√Sm*Gd, where N refers to a chondrite-normalised value (McDonough and Sun, 1995).

Major oxides	Limestone							
(wt.%)	GUZ-9A	GKA-10	KIS-7	KIS-8	AK-11	AK-12	AK-13	Mean
SiO_2	25.34	2.83	4.57	0.93	11.16	9.58	6.66	8.7
Al_2O_3	5.97	0.41	0.20	0.14	1.15	1.39	0.54	1.4
ΣFe_2O_3	1.63	0.25	0.12	0.16	0.52	0.47	0.22	0.5
MgO	0.82	1.54	0.22	0.24	0.75	0.78	0.82	0.7
CaO	34.70	52.34	53.18	55.22	46.44	47.54	50.30	48.5
Na_2O	0.83	0.05	0.02	0.02	0.10	0.14	0.03	0.2
K_2O	1.24	0.06	0.02	0.02	0.13	0.17	0.06	0.2
MnO	0.05	<0.01	0.26	0.22	0.38	0.08	0.11	0.2
TiO_2	0.20	0.02	<0.01	<0.01	0.05	0.05	0.02	0.1
P_2O_5	0.05	0.14	0.08	0.05	0.08	0.11	0.09	0.1
LOI	29.1	42.3	41.3	43.0	39.2	39.6	41.1	39.4
Total	99.93	99.95	99.98	99.97	99.96	99.95	99.94	99.95
ppm								
Ba	251	29	22	25	41	59	47	67.7
Be	<1	<1	<1	<1	<1	<1	<1	<1
Co	4.6	0.8	1.3	0.6	3.0	2.1	1.3	2.0
Cs	6.0	0.3	0.5	0.3	1.4	1.1	0.7	1.5
Ga	6.3	<0.5	<0.5	<0.5	1.5	1.3	0.6	2.4
Hf	1.9	<0.1	<0.1	<0.1	0.4	0.3	0.1	0.7
Nb	4.9	0.4	0.2	<0.1	0.7	0.8	0.3	1.2
Rb	48.7	2.7	2.1	1.4	14.2	12.1	4.9	12.3
Sn	<1	<1	<1	<1	<1	<1	<1	<1
Sr	124.9	117.2	99.4	156.4	160.0	186.2	257.7	157.4
Ta	0.4	<0.1	<0.1	<0.1	<0.1	<0.1	<0.1	0.4
Th	9.8	0.3	<0.2	<0.2	0.4	1.2	0.5	2.4
U	2.3	1.1	1.4	2.2	0.7	1.6	3.5	1.8
V	29	31	48	16	21	30	36	30.1
W	1.6	<0.5	<0.5	<0.5	<0.5	<0.5	<0.5	1.6
Zr	68.3	4.8	4.3	3.2	13.5	14.6	9.0	16.8
Y	15.5	0.8	0.3	0.2	0.8	1.9	0.6	2.9
Mo	0.2	<0.1	0.2	0.2	0.3	0.4	0.4	0.3
Cu	6.1	0.4	1.6	1.1	1.6	4.9	2.6	2.6
Pb	5.7	0.4	0.2	0.2	0.7	1.5	1.0	1.4
Zn	14	1	3	2	3	5	4	4.6
Ni	17.1	2.1	8.1	6.0	8.7	13.3	14.4	10.0
As	6.2	8.2	8.3	9.8	6.7	10.0	8.2	8.2
Cd	1.8	<0.1	0.2	<0.1	0.2	<0.1	<0.1	0.7
Sb	0.2	<0.1	<0.1	<0.1	<0.1	<0.1	<0.1	0.2
Bi	0.1	<0.1	<0.1	<0.1	<0.1	<0.1	<0.1	0.1
Au (ppb)	<0.5	<0.5	0.5	<0.5	<0.5	0.7	1.5	0.9
Hg	<0.01	<0.01	0.02	0.03	<0.01	<0.01	<0.01	0.0
La	19.0	1.3	0.3	0.3	1.1	2.0	0.6	3.5
Ce	24.4	1.9	0.5	0.6	1.7	3.9	1.2	4.9
Pr	3.44	0.22	0.06	0.05	0.18	0.41	0.11	0.6
Nd	12.2	0.6	<0.3	<0.3	0.7	1.4	0.4	3.1
Sm	2.23	0.12	0.05	<0.05	0.12	0.34	0.09	0.5
Eu	0.48	0.03	<0.02	<0.02	0.03	0.08	0.02	0.1
Gd	1.96	0.21	<0.05	<0.05	0.15	0.36	0.09	0.6
Tb	0.35	0.04	<0.01	<0.01	0.02	0.05	0.01	0.1
Dy	2.13	0.12	<0.05	<0.05	0.15	0.32	0.08	0.6
Ho	0.47	0.05	<0.02	<0.02	0.02	0.06	<0.02	0.2
Er	1.40	0.04	<0.03	<0.03	0.09	0.19	0.05	0.4
Tm	0.21	0.03	<0.01	<0.01	0.01	0.03	<0.01	0.1
Yb	1.58	0.16	<0.05	<0.05	0.10	0.21	0.07	0.4
Lu	0.25	0.02	<0.01	<0.01	0.01	0.03	<0.01	0.1
ΣREE	85.6	5.64	1.76	1.75	5.18	11.28	3.36	18.1
ΣLREE	59.04	4.02	1.16	1.25	3.68	7.71	2.31	12.1
ΣMREE	7.62	0.57	0.2	0.2	0.49	1.21	0.31	2.1
ΣHREE	3.44	0.25	0.1	0.1	0.21	0.46	0.14	1
Eu_N/Eu^*	0.70	0.58	1.22	1.22	0.68	0.70	0.68	0.56

Table 3. (continued).

Major oxides (wt.%)	Calcrete					
	SAH-10	SAH-18	S-3	GKA-3	GUZ-3C	Mean
SiO_2	29.88	36.02	39.25	34.43	24.62	32.8
Al_2O_3	7.77	8.33	11.02	9.62	8.16	9.0
ΣFe_2O_3	2.88	2.38	3.73	3.02	3.41	3.1
MgO	1.87	1.23	1.52	1.63	1.49	1.5
CaO	28.10	25.89	21.48	25.55	31.41	26.5
Na_2O	0.61	1.10	1.08	1.06	0.52	0.9
K_2O	0.96	1.47	1.05	1.02	0.93	1.1
MnO	0.14	0.13	0.08	0.05	0.03	0.1
TiO_2	0.31	0.25	0.42	0.36	0.37	0.3
P_2O_5	0.08	0.07	0.11	0.16	0.07	0.1
LOI	27.2	23.0	20.1	23.0	28.9	24.4
Total	99.80	99.87	99.84	99.90	99.91	99.9
ppm						
Ba	227	339	280	232	164	248.4
Be	<1	<1	<1	1	<1	1.0
Co	14.7	6.7	10.1	8.2	9.6	9.9
Cs	2.1	19.1	1.9	6.5	7.7	7.5
Ga	7.7	8.4	11.0	9.1	9.6	9.2
Hf	1.9	1.8	2.6	2.5	2.1	2.2
Nb	6.2	6.9	6.3	6.8	8.1	6.9
Rb	48.4	83.4	52.9	48.3	50.5	56.7
Sn	<1	<1	<1	1	1	1.0
Sr	150.0	176.7	201.4	188.5	128.4	169.0
Ta	0.5	0.5	0.5	0.6	0.4	0.5
Th	6.4	10.6	7.9	9.6	6.3	8.2
U	1.4	2.7	1.5	1.7	1.8	1.8
V	67	36	61	58	78	60.0
W	4.6	1.9	1.1	1.4	1.6	2.1
Zr	70.2	71.3	93.5	76.9	83.7	79.1
Y	24.9	12.0	17.6	11.4	10.3	15.2
Mo	0.3	0.1	0.2	0.3	0.8	0.3
Cu	11.4	10.0	12.4	11.5	13.5	11.8
Pb	9.7	4.1	6.7	9.5	8.5	7.7
Zn	16	13	20	24	31	20.8
Ni	13.4	10.0	13.3	17.7	34.6	17.8
As	3.9	4.8	5.6	7.9	10.0	6.4
Cd	0.2	<0.1	0.3	0.7	0.3	0.4
Sb	<0.1	<0.1	<0.1	0.1	0.2	0.2
Bi	0.1	<0.1	0.1	0.3	0.2	0.2
Au (ppb)	<0.1	<0.1	<0.1	<0.1	<0.1	<0.1
Hg	<0.5	<0.5	<0.5	1.0	<0.5	1.0
La	28.1	17.3	19.3	18.0	16.4	19.8
Ce	38.7	28.4	32.4	31.1	27.0	31.5
Pr	5.49	3.22	3.76	3.59	3.23	3.9
Nd	21.3	11.1	14.3	13.9	11.8	14.5
Sm	3.55	1.95	2.29	2.33	2.03	2.4
Eu	0.81	0.43	0.64	0.55	0.47	0.6
Gd	3.49	1.74	2.36	2.06	1.84	2.3
Tb	0.60	0.31	0.41	0.34	0.29	0.4
Dy	3.69	1.71	2.45	1.98	1.76	2.3
Ho	0.80	0.38	0.52	0.38	0.37	0.5
Er	2.61	1.19	1.53	1.25	1.07	1.5
Tm	0.35	0.15	0.20	0.16	0.14	0.2
Yb	2.79	1.16	1.61	1.20	1.10	1.6
Lu	0.41	0.18	0.25	0.18	0.18	0.2
ΣREE	137.59	81.22	99.62	88.42	77.98	96.9
ΣLREE	93.59	60.02	69.76	66.59	58.43	69.7
ΣMREE	12.94	6.52	8.67	7.64	6.76	8.5
ΣHREE	6.16	2.68	3.59	2.79	2.49	3.5
Eu_N/Eu^*	0.70	0.71	0.84	0.77	0.74	0.78

Table 3. (continued).

Major oxides (wt.%)	Palaeosol						
	SAH-19	S-2	S-5	S-9A	SA-2	GKA-6	Mean
SiO_2	62.82	67.28	64.03	56.83	45.55	51.34	58.0
Al_2O_3	14.99	12.48	13.88	16.76	11.99	15.26	14.2
ΣFe_2O_3	3.82	4.34	5.17	6.44	4.40	5.42	4.9
MgO	1.49	2.02	1.89	3.04	2.64	2.10	2.2
CaO	3.93	4.31	4.38	2.88	14.50	7.73	6.3
Na_2O	2.34	1.26	1.31	1.12	0.87	0.92	1.3
K_2O	2.82	1.06	1.09	1.72	1.42	1.80	1.7
MnO	0.08	0.09	0.09	0.09	0.13	0.04	0.1
TiO_2	0.40	0.47	0.55	0.63	0.46	0.59	0.5
P_2O_5	0.04	0.06	0.07	0.04	0.05	0.10	0.1
LOI	7.1	6.5	7.4	10.3	17.8	14.5	10.6
Total	99.83	99.87	99.86	99.85	99.81	99.80	99.9
ppm							
Ba	469	388	367	172	281	307	330.7
Be	1	<1	<1	<1	<1	<1	1.0
Co	8.4	12.9	14.5	13.0	16.5	11.0	12.7
Cs	45.4	2.2	2.1	2.9	3.3	25.2	13.5
Ga	13.5	13.6	14.0	17.6	11.6	14.9	14.2
Hf	3.6	2.8	3.0	3.6	2.7	3.3	3.2
Nb	10.9	7.5	8.7	9.9	8.6	13.1	9.8
Rb	151.6	51.8	59.7	73.5	66.2	111.0	85.6
Sn	1	<1	1	2	1	2	1.4
Sr	232.5	222.5	252.2	164.6	146.1	138.9	192.8
Ta	0.9	0.5	0.6	0.6	0.6	1.0	0.7
Th	18.2	8.4	10.5	8.7	9.4	14.8	11.7
U	4.4	6.8	2.2	2.6	1.2	2.7	3.3
V	59	81	103	89	70	127	88.2
W	2.7	1.1	1.2	2.4	4.7	1.5	2.3
Zr	117.2	100.0	110.8	127.8	98.4	112.6	111.1
Y	14.9	24.0	19.0	41.3	20.8	17.5	22.9
Mo	0.4	0.3	0.2	0.2	<0.1	0.2	0.3
Cu	15.6	21.6	18.7	15.0	15.0	19.2	17.5
Pb	6.1	5.8	7.6	7.7	11.8	15.2	9.0
Zn	27	27	32	36	24	55	33.5
Ni	14.1	13.8	17.0	20.1	17.3	28.6	18.5
As	2.5	5.5	5.2	4.1	2.8	4.2	4.1
Cd	<0.1	<0.1	<0.1	0.20	0.10	<0.1	0.2
Sb	0.1	<0.1	<0.1	<0.1	<0.1	<0.1	0.1
Bi	0.1	0.1	0.2	0.2	0.2	0.4	0.2
Au (ppb)	<0.5	<0.5	<0.5	<0.5	<0.5	<0.5	0.5
Hg	<0.01	<0.01	<0.01	<0.01	<0.01	0.01	0.01
La	25.2	22.3	22.7	32.3	29.4	27.3	26.5
Ce	45.9	32.8	39.5	33.9	46.4	56.5	42.5
Pr	4.59	4.95	4.92	7.01	5.87	6.20	5.6
Nd	16.4	18.6	18.0	26.8	22.2	23.6	20.9
Sm	2.71	3.50	3.28	4.98	3.72	4.10	3.7
Eu	0.66	0.87	0.82	1.30	0.89	0.91	0.9
Gd	2.28	3.41	2.98	5.28	3.63	3.55	3.5
Tb	0.41	0.60	0.50	0.98	0.62	0.59	0.6
Dy	2.47	3.50	2.86	6.19	3.63	3.27	3.7
Ho	0.52	0.75	0.58	1.26	0.78	0.63	0.8
Er	1.55	2.22	1.79	3.99	2.22	1.80	2.3
Tm	0.21	0.31	0.24	0.56	0.31	0.23	0.3
Yb	1.61	2.41	1.83	4.11	2.36	1.82	2.4
Lu	0.26	0.36	0.29	0.67	0.35	0.26	0.4
ΣREE	119.67	120.58	119.29	170.63	143.18	148.26	137
ΣLREE	92.09	78.65	85.12	100.01	103.87	113.6	95.5
ΣMREE	9.05	12.63	11.02	19.99	13.27	13.05	13.2
ΣHREE	3.63	5.3	4.15	9.33	5.24	4.11	5.4
Eu_N/Eu^*	0.81	0.77	0.80	0.77	0.74	0.73	0.76

Table 3. (continued).

Major oxides (wt.%)	Fluvial			Diatomite			Pyroclast		
	SA-4	GKA-8	Mean	SAH-1	GUZ-7	Mean	SAH-8	SAH-16	Mean
SiO_2	61.82	55.69	58.76	60.62	52.34	56.48	55.82	60.48	58.15
Al_2O_3	14.44	14.59	14.52	12.36	14.98	13.67	12.59	14.89	13.74
ΣFe_2O_3	4.34	6.06	5.20	4.55	4.84	4.70	3.49	4.05	3.77
MgO	2.27	6.10	4.19	2.24	2.49	2.37	1.65	1.82	1.74
CaO	2.53	7.80	5.17	4.71	7.34	6.03	11.59	4.48	8.04
Na_2O	1.12	2.01	1.57	0.96	1.01	0.99	2.00	1.85	1.93
K_2O	1.96	1.18	1.57	1.80	1.35	1.58	1.73	1.47	1.6
MnO	0.07	0.08	0.08	0.04	0.06	0.05	0.09	0.12	0.11
TiO_2	0.48	0.68	0.58	0.44	0.65	0.55	0.36	0.44	0.4
P_2O_5	0.05	0.10	0.08	0.04	0.17	0.11	0.07	0.06	0.07
LOI	10.8	5.4	8.10	12.0	14.6	13.30	10.4	8.9	9.7
Total	99.88	99.69	99.82	99.76	99.83	99.83	99.83	99.81	99.82
ppm									
Ba	316	456	386	300	274	287	447	512	480
Be	1	<1	1	1	<1	1	<1	1	1
Co	7.4	15.2	11.3	8.8	15.9	12.4	11.5	12.2	11.9
Cs	4.3	5.4	4.9	6.7	13.8	10.3	2.8	4.6	3.7
Ga	13.1	14.1	13.6	12.6	16.9	14.8	11.8	8.4	10.1
Hf	3.8	2.7	3.3	3.6	3.3	3.5	2.6	1.8	2.2
Nb	12.9	7.0	10.0	11.4	12.2	11.8	6.8	6.9	6.9
Rb	97.6	45.9	71.8	91.2	89.7	90.5	68.1	83.4	75.8
Sn	2	1	2	3	2	3	2	<1	2
Sr	147.4	382.8	265.1	245.1	191.5	218.3	222.1	176.7	199.4
Ta	1.0	0.4	0.7	0.9	1.0	1.0	0.6	0.5	0.6
Th	15.9	6.7	11.3	15.4	12.6	14.0	7.9	10.6	9.3
U	2.4	1.2	1.8	3.5	2.2	2.9	2.0	2.7	2.4
V	61	150	106	443	170	307	91	36	63.5
W	3.2	0.7	2.0	1.7	2.9	2.3	2.6	1.9	2.25
Zr	120.8	92.9	106.9	131.0	150.4	140.7	97.7	71.3	84.5
Y	15.4	15.9	15.7	14.5	25.8	20.2	16.9	12.0	14.5
Mo	0.2	0.2	0.2	0.5	0.2	0.4	0.2	0.1	0.15
Cu	17.4	17.4	17.4	21.5	32.5	27.0	8.7	10.0	9.4
Pb	10.5	5.3	7.9	13.9	13.6	13.8	5.6	4.1	4.9
Zn	29	34	32	31	64	48	19	13	16
Ni	13.3	14.1	13.7	28.3	45.1	36.7	10.3	10.0	10.2
As	2.5	5.6	4.1	2.3	3.0	2.7	2.2	4.8	3.5
Cd	<0.1	<0.1	<0.1	<0.1	0.1	0.1	<0.1	<0.1	<0.1
Sb	<0.1	<0.1	<0.1	<0.1	0.1	0.1	<0.1	<0.1	<0.1
Bi	<0.1	<0.1	<0.1	0.2	0.4	0.3	<0.1	<0.1	<0.1
Au (ppb)	0.3	<0.1	0.2	<0.5	<0.5	<0.5	<0.1	<0.1	<0.1
Hg	1.6	<0.5	1.1	<0.01	<0.01	<0.01	1.0	<0.5	1
La	26.6	18.0	22	29.1	32.5	30.8	19.6	17.3	18.5
Ce	52.1	38.5	45	52.7	52.9	52.8	33.7	28.4	31.1
Pr	5.42	4.51	4.97	5.99	7.47	6.73	3.98	3.22	3.6
Nd	18.9	18.8	18.9	22.3	28..7	25.5	15.7	11.1	13.4
Sm	3.15	3.35	3.25	3.32	5.14	4.23	2.61	1.95	2.28
Eu	0.67	0.91	0.79	0.71	1.14	0.93	0.73	0.43	0.58
Gd	2.83	3.20	3.02	2.80	4.74	3.77	2.55	1.74	2.15
Tb	0.49	0.51	0.50	0.46	0.76	0.61	0.43	0.31	0.37
Dy	2.73	2.81	2.77	2.46	4.26	3.36	2.56	1.71	2.14
Ho	0.57	0.56	0.57	0.50	0.84	0.67	0.57	0.38	0.48
Er	1.62	1.61	1.62	1.49	2.57	2.03	1.58	1.19	1.39
Tm	0.21	0.22	0.22	0.22	0.34	0.28	0.23	0.15	0.19
Yb	1.73	1.47	1.60	1.63	2.60	2.12	1.64	1.16	1.40
Lu	0.24	0.22	0.23	0.24	0.39	0.32	0.26	0.18	0.22
ΣREE	132.66	110.57	121.14	138.42	170.15	154.35	103.04	81.22	92.3
ΣLREE	103.02	79.81	90.87	110.09	121.57	115.83	72.98	60.02	66.6
ΣMREE	10.44	11.34	10.9	10.25	16.88	13.57	9.45	6.52	8
ΣHREE	3.8	3.52	3.67	3.58	5.9	4.75	3.71	2.68	3.2
Eu_N/Eu^*	0.68	0.85	0.77	0.71	0.70	0.71	0.86	0.71	0.80

Table 3. (continued).

Major oxides (wt.%)	Ignimbrite				Basement rocks
	▲ Cemilköy	▲ Gördeles	▲ Kızılkaya	Mean	*gabbro
SiO_2	73.16	68.82	47.81	71.80	47.81
Al_2O_3	12.62	14.58	16.34	13.32	16.34
ΣFe_2O_3	1.00	2.30	7.41	1.55	7.41
MgO	0.28	0.72	10.25	0.44	10.25
CaO	0.95	2.14	14.79	1.46	14.79
Na_2O	2.26	2.90	1.46	2.75	1.46
K_2O	5.47	5.42	0.09	5.19	0.09
MnO	0.06	0.08	0.13	0.06	0.13
TiO_2	0.11	0.30	0.28	0.21	0.28
P_2O_5	0.03	0.08	0.02	0.05	0.02
LOI	3.29	2.95	1.30	2.92	1.30
Total	99.23	100.28	99.88	99.76	99.88
ppm					
Ba	785.5	656.7	148	706.87	148
Be	–	–	–	-	–
Co	3.8	2.6	<50	3.47	<50
Cs	–	–	–	-	–
Ga	12.7	13.3	–	12.9	–
Hf	–	–	–	-	–
Nb	8.6	17.0	<10	11.23	<10
Rb	203.6	186.2	6	194.3	6
Sn	–	–	–	-	–
Sr	81.3	174.4	115	127.7	115
Ta	–	–	<50	-	<50
Th	–	–	–	-	–
U	–	–	–	-	–
V	6.8	20.6	–	13.17	–
W	–	–	–	-	–
Zr	95.6	236.7	22	156.9	22
Y	9.7	25.4	<10	14.73	<10
Mo	–	–	–	-	–
Cu	–	–	116	-	116
Pb	–	–	–	-	–
Zn	–	–	<50	-	<50
Ni	7.4	8.6	122	13.37	122
As	–	–	–	-	–
Cd	–	–	–	-	–
Sb	–	–	–	-	–
Bi	–	–	–	-	–
Au (ppb)	–	–	–	-	–
Hg	–	–	–	-	–
La	29.43	35.58	0.60	32.09	0.60
Ce	48.94	61.01	0.50	52.73	0.50
Pr	3.83	5.67	<0.20	4.43	<0.20
Nd	12.91	18.99	1.20	14.51	1.20
Sm	2.31	3.24	0.60	2.41	0.60
Eu	0.32	0.61	0.40	0.43	0.40
Gd	1.77	2.88	0.60	2.02	0.60
Tb	–	–	<0.20	-	<0.20
Dy	1.85	2.89	0.50	2.05	0.50
Ho	–	–	0.50	-	0.50
Er	1.37	2.08	1	1.53	1
Tm	–	–	0.40	-	0.40
Yb	1.58	2.34	0.50	1.74	0.50
Lu	0.25	0.38	0.20	0.28	0.20
ΣREE	114.26	161.07	17.4	128.96	17.4
ΣLREE	95.11	121.25	2.5	103.77	2.5
ΣMREE	6.25	9.62	2.8	8.10	2.8
ΣHREE	3.2	4.8	2.1	3.56	2.1
Eu_N/Eu^*	0.48	0.61	2.03	0.61	2.03

Data sources: * = Işık et al.,(2002), ▲= Temel (1992).

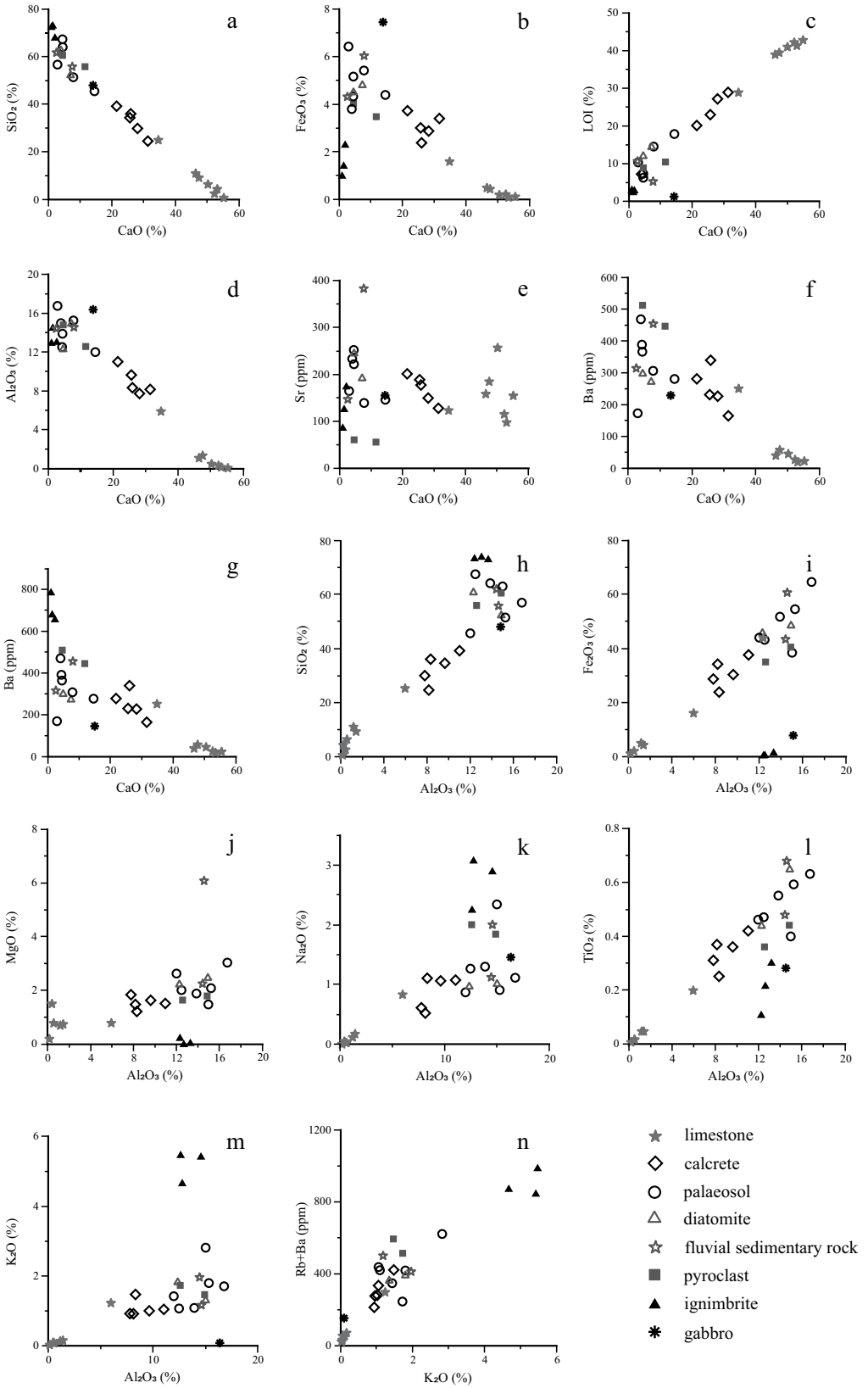

Figure 8. Elemental variation diagrams for major oxides (wt.%) and trace elements (ppm), plotted versus CaO, Al_2O_3, and K_2O, for samples from the study area.

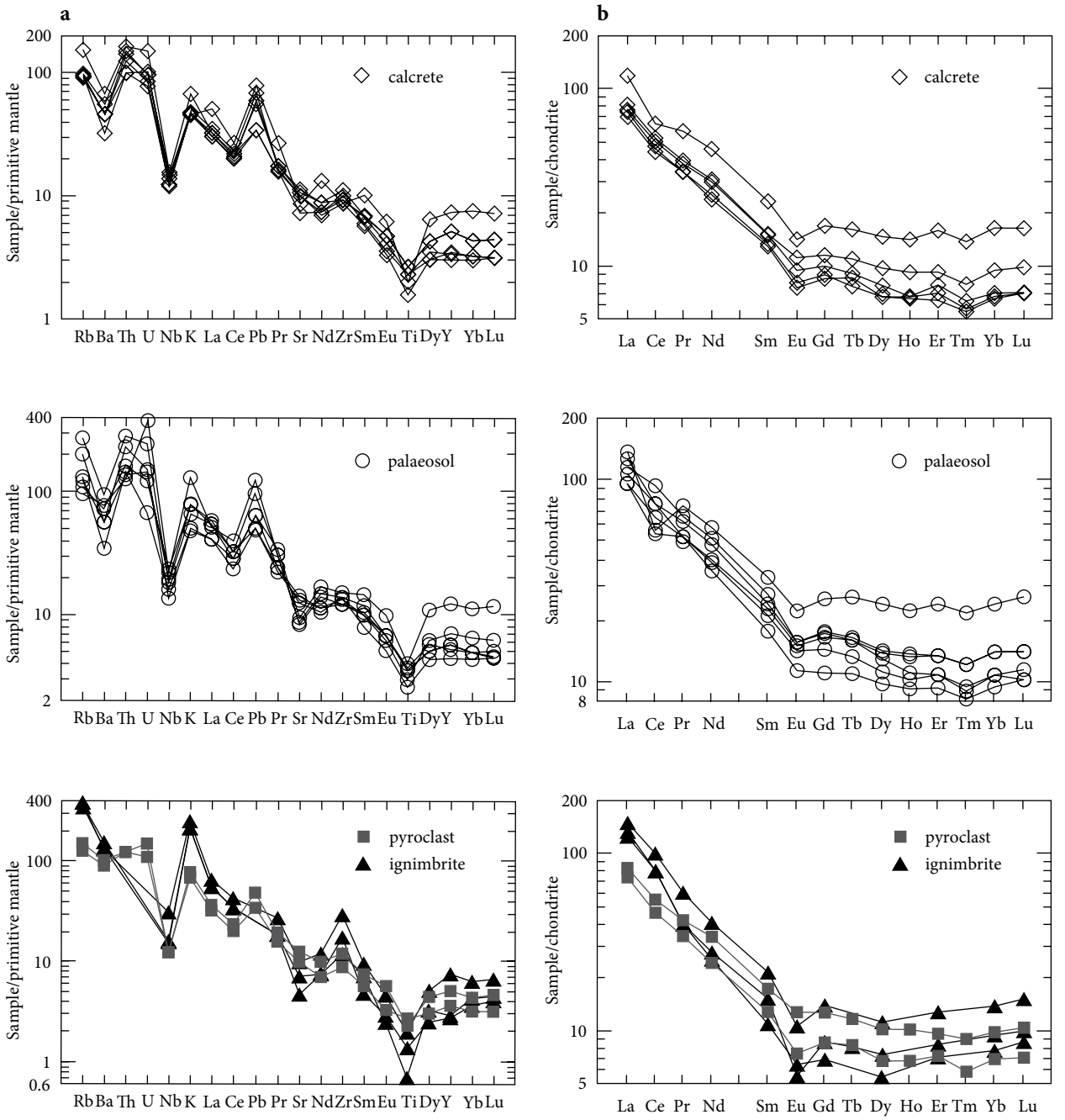

Figure 9. (a) Primitive-mantle- (Taylor and McLennan, 1985) and **(b)** chondrite- (Boynton, 1984) normalised spider diagrams of the calcrete, palaeosol, pyroclast, and ignimbrite.

Toprak, 2010). Görür et al. (1995) and Akgün et al. (1995) also emphasised that a warming trend in the Late Miocene sedimentary successions of central Anatolia shows a fluctuation of dry and wet-warm periods based on pollen assemblages. The calcretes in and/or on palaeosols consist predominantly of calcite associated with quartz, feldspar, and accessory smectite ± palygorskite. The presence of fibrous palygorskite on calcite crystals and at the edges of smectite plates suggests that the palygorskite formed authigenically through the high Si and Mg and low Al ion activities originating from the degradation of volcanic materials and smectitic clays under the predominantly arid or seasonally arid climatic conditions. These conditions controlled the strongly evaporated percolating groundwater during or following calcite precipitation in a vadose zone (Suárez et al., 1994; Sánchez and Galán, 1995;

Table 4. Molecular alteration ratios of ignimbrite and fluvial-lacustrine sedimentary rock samples (profiles P1–P7).

Sample #	Na_2O/K_2O	$CaO+MgO/Al_2O_3$	Al_2O_3/SiO_2	$Al_2O_3/(CaO+MgO+Na_2O+K_2O)$	Ba/Sr
GUZ-9a	0.67	5.95	0.24	0.16	2.01
GKA-10	0.83	131.41	0.14	0.01	0.25
KIS-7	1.00	267.00	0.04	0.01	0.22
KIS-8	1.00	396.14	0.15	0.01	0.16
AK-11	0.77	41.03	0.10	0.02	0.26
AK-12	0.82	34.76	1.15	0.03	0.32
AK-13	0.5	94.67	0.08	0.01	0.18
SAH-10	0.64	3.86	0.26	0.25	1.51
SAH-18	0.75	3.26	0.23	0.28	1.92
S-3	1.03	2.09	0.28	0.44	1.39
GKA-3	1.04	2.83	0.28	0.33	1.23
GUZ-3C	0.56	4.03	0.33	0.24	1.28
SAH-19	0.83	0.36	0.24	1.42	2.02
S-2	1.19	0.51	0.19	1.44	1.74
S-5	1.20	0.45	0.22	1.60	1.46
S-9A	0.65	0.35	0.29	1.91	1.04
SA-2	0.61	1.43	0.26	0.61	1.92
GKA-6	0.51	0.64	0.30	1.22	2.21
SA-4	0.57	0.33	0.23	1.83	2.14
GKA-8	1.70	0.95	0.26	0.85	1.19
SAH-1	0.53	0.56	0.20	1.27	1.22
GUZ-7	0.75	0.66	0.29	1.23	1.43
SAH-8	1.16	1.05	0.23	0.74	2.01
SAH-16	1.26	0.42	0.25	1.55	2.90
Cemilköy	0.41	0.10	0.17	1.41	9.66
Gördeles	0.54	0.20	0.21	1.30	3.77
Kızılkaya	0.66	0.13	0.17	1.36	5.32

Table 5. Standard indicator of palaeosols based on the classification and geochemistry (Soil Survey Staff, 1998).

Molar ratio	Indicator	Normal value	Strong effect
Na_2O/K_2O	Salting	<1	>1
$CaO+MgO/Al_2O_3$	Calcification	<2	>10
Al_2O_3/SiO_2	Formation of clays	0.1–0.3	>0.3
$Al_2O_3/CaO+MgO+Na_2O+K_2O$	Hydrolisation	<2	>100
Ba/Sr	Podzolisation (leaching)	~2	>10

Verrecchia and Le Coustumer, 1996; Colson et al., 1998; Galán and Pozo, 2011; Yalçın and Bozkaya, 2011).

The palaeosol samples are characterised by high Al_2O_3, Fe_2O_3, and SiO_2, all related to the presence of feldspar and smectite in the samples (Gürel and Kadir, 2006). An increasing correlation between Al_2O_3 and SiO_2 associated with elevated smectite and feldspar contents in the source rocks has been reported for Pliocene fluvial lacustrine deposits in the central part of the CVP (Gürel and Kadir, 2006) and in Kalahari duricrusts of the Moshaweng dry valleys in Botswana (Kampunzu et al., 2007). The molecular alteration ratio of fluvial, lacustrine,

Table 6. $\delta^{13}C$ and $\delta^{18}O$ values of limestone and calcrete samples from the Kışladağ and Bayramhacılı members.

	Sample	Rock type	$\delta^{18}O$ ‰	$\delta^{13}C$ ‰
	P2			
Pliocene	GKA-11	Limestone	–8.80	1.54
	GKA-10	Limestone	–8.71	3.37
	GKA-9	Limestone	–9.77	5.71
	P3*			
Pliocene	*GUZ- 10C	Limestone	–10.71	1.81
	*GUZ-10B	Limestone	–10.51	1.78
	*GUZ-10A	Limestone	–10.51	1.85
	*GUZ-3C	Calcrete	–9.13	4.97
	*GUZ-3B	Calcrete	–9.13	4.97
	*GUZ-3A	Calcrete	–9.13	4.97
	*GUZ-2C	Calcrete	–10.00	3.80
	*GUZ-2B	Calcrete	–10.05	3.80
	*GUZ-2A	Calcrete	–10.02	3.80
	*GUZ-1C	Calcrete	–10.64	3.06
	*GUZ-1B	Calcrete	–10.69	3.00
	*GUZ-1A	Calcrete	–10.60	3.03
	P6			
Pliocene	AK-13	Limestone	–9.17	4.05
	AK-12	Limestone	–9.28	1.11
	AK-11	Limestone	–9.99	5.26
	P5			
Pliocene	KIS-8	Limestone	–9.81	2.62
	KIS-7	Limestone	–10.00	3.26
	P4			
Late Miocene	SAH-13	Limestone	–9.68	-0.84
	SAH-11	Limestone	–9.75	-1.97

Data source: * = Gürel (2009).

and volcano-sedimentary rocks (Table 5) also suggests that the region has undergone continuous erosion, resulting in normal salting, calcification, and the formation of clay minerals by hydrolysis, and a leaching mechanism. Thus, the weathering of volcanic materials would be the main source in the development of palaeosols in the CVP. In contrast, the presence of aridisols associated with calcretes indicates arid and semiarid climatic conditions in the region (Khadkikar et al., 1998, 2000).

The high Rb, Ba, and Sr values in the calcretes and the general inverse relationship of CaO with Sr and Ba suggest that the calcretes developed within the palaeosol horizons and that the major- and trace-element budgets of both the soils and the calcretes reflects, to the first order, those of the bedrock, which experienced chemical weathering coeval with soil formation in the fluvial floodplain deposits. Similar negative anomalies for Ba, Nb, Ce, Sr, and Ti; the parallel REE profiles of the palaeosol, calcrete, pyroclast, and ignimbrite samples; the enrichment of LREEs relative to the MREEs and HREEs; and the negative Eu anomaly all suggest that the formation of the palaeosols and calcretes benefited from the alteration of amphibole and plagioclase on/in volcanogenic materials (Braide and Huff, 1986; Gürel, 1991; Rollinson, 1993). The alteration process(es) of these materials resulted from the influence of groundwater during pedogenesis. The relatively high SiO_2 and Ba/Sr contents of both the palaeosols and the calcretes suggest an influx of volcanic material, which is also supported by petrographic data.

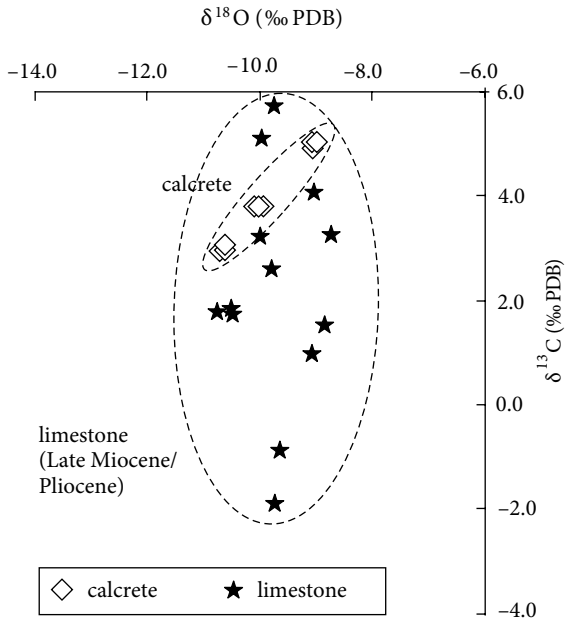

Figure 10. Cross-plot of $\delta^{18}O$ versus $\delta^{13}C$ values showing the distribution of the lacustrine limestone and calcrete samples.

The $\delta^{18}O$ values of the limestones and calcretes are almost identical and vary within a narrow range (Table 6; Figure 10). These more negative $\delta^{18}O$ values (–8.71‰ to –10.71‰ V-PDB) reflect the meteoric water under the influence of high-elevation precipitation (Xu et al., 2013). Similar $\delta^{18}O$ values, ranging from –8‰ to –12‰ SMOW and –9.99‰ to –11.28‰ SMOW, were obtained by Lüdecke et al. (2013) for present-day meteoric waters on the plateau in central Anatolia and by Yıldız et al. (2008) in a neighbouring area, respectively. In Figure 10, the $\delta^{18}O$ values of the calcrete samples are similar to those of the lacustrine carbonate samples, indicating deposition in a shallow lake or at the lake margin, where carbonates were affected by subaerial exposure. Therefore, these values reflect not only the sedimentary but also the pedogenic and/or diagenetic environment (Wright and Platt, 1995). Ostracods and gastropods in the micritic limestones reflect very low energy conditions. Despite the isotopic similarity, the lacustrine carbonates are differentiated from calcrete samples by their fossil content and bedding characteristics. The calcretes are nodular, tubular, massive, and fracture infilling in and/or on palaeosols. The $\delta^{18}O$ values of the lacustrine carbonates provide evidence of the hydrologic conditions, in terms of evaporative enrichment and water inflow. The absence of covariance between $\delta^{18}O$ and $\delta^{13}C$ values in Figure 10 suggests a hydrologically open lake system (Talbot, 1990). The lake was fed by surface and groundwater.

The $\delta^{13}C$ isotope values of the limestones and calcretes vary over a wider range (from –1.97‰ to 5.71‰) than the $\delta^{18}O$ values. These values reflect the changing conditions in the lake system. The main factors determining the carbon isotope value of the lake water are the isotopic composition of the inflowing water, the level of biotic productivity, the atmospheric exchange, and the residence time (Talbot and Kelts, 1990; Bristow et al., 2012). Under isotopic equilibrium with atmospheric CO_2, which normally has a $\delta^{13}C$ value of –8‰, lake water $\delta^{13}C$ values would be between 1‰ and 3‰ (Leng and Marshall, 2004). Therefore, positive $\delta^{13}C$ values of lacustrine carbonates, as well as calcretes, indicate precipitation from lake and surface water or groundwater under isotopic equilibrium with atmospheric CO_2 (Botz and Von Der Borch, 1984). Calcretes with positive $\delta^{13}C$ values indicate a pedogenic environment with low plant respiration and a predominance of C_4 plants (Harrison et al., 1993; Eren, 2011). Certain lacustrine limestone samples have slightly negative $\delta^{13}C$ values despite stable $\delta^{18}O$ values, and these samples show high Ba/Sr values. Therefore, these values are due to increased water depth in the lake, indicating a significant input of most likely surface water that was strongly influenced by the weathering products of ignimbrites with high Ba/Sr values.

The major outcomes of this study can be summarised as follows:

(1) The lake was filled by pyroclastic and siliciclastic fluvial sediments and intercalated with limestones, marlstone, and diatomites.

(2) The presence of palaeosols and calcretes indicates surface or near-surface conditions. The palaeosols mainly comprise smectite ± illite with feldspar, quartz, calcite, opal-CT, and amphibole. The calcretes are composed predominantly of calcite, accompanied by minor feldspar, quartz, and accessory smectite ± palygorskite.

(3) Micromorphologically, palygorskite formation on/between calcite and at the edge of smectite indicates a direct precipitation from relatively more evaporated Si- and Mg-rich and Al-poor water in an alkaline environment.

(4) The alteration of ignimbrites resulted in the consumption of SiO_2, Al_2O_3+Fe_2O_3, TiO_2, and K_2O by the precipitation of smectite ± illite in palaeosols and of CaO by calcite in calcretes during pedogenesis.

(5) The high Ba/Sr ratios; the negative anomalies for Ba, Nb, Ce, Sr, and Ti; the enrichment of LREEs relative to the MREEs and HREEs; and a negative Eu anomaly in palaeosols, calcretes, pyroclasts, and ignimbrite samples likely reflect crystal fractionation of feldspar and amphibole, as well as syngenetic soil formation from the alteration of volcaniclastic source rocks.

(6) The $\delta^{18}O$ values of the calcretes and limestones indicate precipitation from meteoric water at high elevation. The positive $\delta^{13}C$ values of the limestones exhibit calcite precipitation in isotopic equilibrium with the lake water. The slightly negative $\delta^{13}C$ values of certain limestone

samples may indicate deposition during periods with higher surface or groundwater contributions. The high positive $\delta^{13}C$ values of calcretes indicate a predominance of C_4 plants.

Acknowledgements
This research constitutes further work from the first author's MSc study. The authors are indebted to Professor Gierlowski-Kordesch (Ohio University) and 2 anonymous reviewers for their extremely careful and constructive reviews, which significantly improved the quality of the paper. Professor Warren D Huff (University of Cincinnati) is gratefully acknowledged for detailed reviews and suggestions on an early draft of the manuscript.

References

Akgün F, Olgun E, Kuşcu I, Toprak V, Göncüoğlu MC (1995). New data on the stratigraphy, depositional environment, and real age of the Oligo-Miocene cover of the central Anatolian crystalline complex. TPJD Bulletin 6: 51–68 (in Turkish with English abstract).

Atabey E, Atabey N, Kara H (1998). Kırşehir yöresi kaliş (kalkrit) oluşumlarının sedimantolojisi. MTA Dergisi 120: 93–104 (in Turkish).

Aydar E, Schmitt AK, Çubukçu HE, Akin L, Ersoy O, Sen E, Duncan RA, Atici G (2012). Correlation of ignimbrites in the central Anatolian volcanic province using zircon and plagioclase ages and zircon compositions. J Volcanol Geoth Res 213–214: 83–97.

Beekman PH (1966). Hasandağı-Melendizdağ Bölgelerinde Pliyosen ve Kuvaterner volkanizma faaliyetleri. MTA Dergisi 66: 90–105 (in Turkish).

Bohacs KM, Carroll AR, Neal JE (2003). Lessons from large lake systems - thresholds, nonlinearity, and strange attractors. In: Chan MA, Archer AW, editors. Extreme Depositional Environments: Mega End Members in Geologic Time. Geo Soc Am Spec Paper 370: 75–90.

Bohacs KM, Carroll AR, Neal JE, Mankiewicz PJ (2000). Lake-basin type, source potential, and hydrocarbon character: an integrated sequence-stratigraphic-geochemical framework. In: Gierlowski-Kordesch EH, Kelts KR, editors. Lake Basins Through Space and Time, AAPG Studies in Geology 46. Tulsa, OK, USA: AAPG, pp. 3–33.

Botz, RW, Von Der Borch CC (1984). Stable isotope study of carbonate sediments from the Coorong Area, south Australia. Sedimentology 31: 837–849.

Boynton WV (1984). Cosmochemistry of the rare earth elements: meteorite studies. In: Henderson P, editor. Rare Earth Element Geochemistry. Amsterdam, the Netherlands: Elsevier, pp. 63–114.

Braide SP, Huff WD (1986). Clay mineral variation in Tertiary sediments from the Eastern Flank of the Niger Delta. Clay Miner 21: 211–224.

Brindley GW (1980). Quantitative X-ray analysis of clays. In: Brindley GW, Brown G, editors. Crystal Structures of Clay Minerals and Their X-ray Identification. London, UK: Mineralogical Society Monograph 5, pp. 411–438.

Bristow TF, Kennedy MJ, Morrison KD, Mrofka DD (2012). The influence of authigenic clay formation on the mineralogy and stable isotopic record of lacustrine carbonates. Geochim Cosmochim Ac 90: 64–82.

Colson J, Cojan I, Thiry M (1998). A hydrogeological model for palygorskite formation in the Danian continental facies of the Provence Basin (France). Clay Miner 33: 333-347.

Dirik K (2001). Neotectonic evolution of the northwestward arched segment of the Central Anatolian Fault Zone, Central Anatolia, Turkey. Geodin Acta 14: 147–158.

Dunham RJ (1962). Classification of carbonate rocks according to depositional texture. In: Ham WE, editor. Classification of Carbonate Rocks. Tulsa, OK, USA: American Association of Petroleum Geologists, pp. 108–121.

Eren M (2011). Stable isotope geochemistry of Quaternary calcretes in the Mersin area, southern Turkey - a comparison and implications for their origin. Chem Erde-Geochem 71: 31–37.

Erol O (1999). A geomorphological study of the Sultansazligi lake, central Anatolia. Quaternary Sci Rev 18: 647–657.

Galán E, Pozo M (2011). Palygorskite and sepiolite deposits in continental environments. Description, genetic patterns and sedimentary settings. In: Galán E, Singer E, editors. Developments in Palygorskite-Sepiolite Research. A New Outlook on these Nanomaterials. Developments in Clay Science, Vol. 3. Amsterdam, the Netherlands: Elsevier, pp. 125–173.

Gierlowski-Kordesch EH, Rust BR (1994). The Jurassic East Berlin Formation, Hartford Basin, Newark Supergroup (Connecticut and Massachusetts): a saline lake/playa/alluvial plain system. In: Renaut RW, Last WM, editors. Sedimentology and Geochemistry of Modern and Ancient Saline Lakes. Tulsa, OK, USA: Society for Sedimentary Geology Special Pub. No. 50, pp. 249–265.

Göncüoğlu C, Toprak V (1992). Neogene and Quaternary volcanism of Central Anatolia: a volcano structural evolution. Bulletin de la Section de Volcanologie Societe Geologique de France 26: 1–6.

Görür N, Sakınç M, Barka A, Akkök R, Ersoy S (1995). Miocene to Pliocene palaeogeographic evolution of Turkey and its surroundings. J Hum Evol 28: 309–324.

Gürel A (1991). Veränderung im Stoffbestand der Verwitterungsdecke als Folge Natüricher Bodenbildungsprozesse und Antropogener atmosphärischer Deposition. PhD, University of Göttingen, Göttingen, Germany (in German).

Gürel A (2009). Clay mineralogy of Neogene sequences of Cappadocian Volcanic Provence (CVP, Central Anatolia): Source of sediment-palaeosols and paleoclimatic variations. YDABCAG–104Y070. Ankara, Turkey: TÜBİTAK (in Turkish with English abstract).

Gürel A, Kadir S (2006). Geology and mineralogy and origin of clay minerals of the Pliocene fluvial-lacustrine deposits in the Cappadocian Volcanic Province, Central Anatolia, Turkey. Clay Clay Miner 54: 555–570.

Gürel A, Kadir S (2008). Geology and mineralogy of Late Miocene clayey sediments in the southeastern part of the Central Anatolian Volcanic Province, Turkey. Clay Clay Miner 56: 307–321.

Gürel A, Kadir S (2010). Palaeoenvironmental approach to the geology, mineralogy and geochemistry of an Early Miocene alluvial-fan to cyclic shallow-lacustrine depositional system in the Aktoprak Basin (central Anatolia), Turkey. Clay Miner 45: 51–75.

Gürel A, Yıldız A (2007). Diatom communities, lithofacies characteristics and paleoenviromental interpretation of Pliocene diatomite deposits in the Ihlara-Selime plain (Aksaray, Central Anatolia, Turkey). J Asian Earth Sci 30: 170–180.

Harrison TM, Copeland P, Hall SA, Quade J, Burner S, Ojha TP, Kidd WSF (1993). Isotopic preservation of Himalayan/Tibetan uplift, denudation, and climatic histories of two Molasse deposits. J Geol 101: 157–175.

Innocenti F, Mazzuoli R, Pasquare G, Radicati Di Brozolo F, Villari L (1975). The Neogene calc-alcaline volcanism of Central Anatolia: geochronological data on Kayseri-Niğde area. Geol Mag 112: 349–360.

Işık F, Baş H, Koçak K (2002). Petrographic and geochemical characteristics of gabbroic rocks: Central Anatolian Massif, Yeşilhisar-Kayseri (Turkey). Pamukkale Üniversitesi Mühendislik Fakültesi Mühendislik Bilimleri Dergisi 8: 227–238 (in Turkish with English abstract).

Kadir S, Gürel A, Senem H, Külah T (2013). Geology of Late Miocene clayey sediments and distribution of palaeosolclay minerals in the northeastern part of the Cappadocian Volcanic Province (Araplı-Erdemli), central Anatolia, Turkey. Turkish J Earth Sci 22: 427–443.

Kampunzu AB, Ringrose S, Huntsman-Mapila P, Harris C, Vink BW, Matheson W (2007). Origins and palaeo-environments of Kalahari duricrusts in the Moshaweng dry valleys (Botswana) as detected by major and trace element composition. J Afr Earth Sci 48: 199–221.

Karakaş Z, Kadir S (1998). Mineralogical and genetic relationships between carbonate and sepiolite-palygorskite formations in the Neogene lacustrine Konya Basin, Turkey. Carbonate Evaporite 13: 198–206.

Khadkikar AS, Chamyal LS, Ramesh R (2000). The character and genesis of calcrete in Late Quaternary alluvial deposits, Gujarat, western India, and its bearing on the interpretation of ancient climates. Palaeogeogr Palaeoclimatol Palaeoecol 162: 239–261.

Khadkikar AS, Merh SS, Malik JN, Chamyal LS (1998). Calcretes in semi-arid alluvial systems: formative pathways and sinks. Sediment Geol 116: 251–260.

Last WM (1994). Climatic and tectonic rhythms in lake deposits: an IGCP Project 324 contribution. J Paleolimnol 11: 1–2.

Leng MJ, Marshall JD (2004). Palaeoclimate interpretation of stable isotope data from lake sediment archives. Quat Sci Rev 23: 811–831.

Le Pennec JL, Bourdier JL, Froger JL, Temel A, Camus G, Gourgaud A (1994). Neogene ignimbrites of the Nevşehir Plateau (Central Anatolia): stratigraphy, distribution and source constraints. J Volcanol Geoth Res 63: 59–87.

Le Pennec JL, Temel A, Froger JL, Sen S, Gourgaud A, Bourdier JL (2005). Stratigraphy and age of the Cappadocia ignimbrites, Turkey: reconciling field constraints with paleontologic, radiochronologic, geochemical and paleomagnetic data. J Volcanol Geoth Res 141: 45–64.

Lüdecke T, Mikes T, Rojay FB, Cosca MA, Mulch A (2013). Stable isotope-based reconstruction of Oligo-Miocene paleoenvironment and paleohydrology of central Anatolai lake basins (Turkey). Turkish J Earth Sci 22: 793–819.

McCrea JM (1950). On the isotopic chemistry of carbonates and a paleotemperature scale. J Chem Phys 18: 849–857.

McDonough WF, Sun S (1995). The composition of the Earth. Chem Geol 120: 223–253.

Miall AD (1996). The Geology of Fluvial Deposits. Sedimentary Facies, Basin Analysis, and Petroleum Geology. Amsterdam, the Netherlands: Springer.

Moore DM, Reynolds RC (1989). X-ray Diffraction and the Identification and Analysis of Clay Minerals. New York, NY, USA: Oxford University Press.

Müller O (1895). Über Achsen, Orientierungs- und Symmetrieebenen bei den Bacillariophyceen. Ber Deut Bot Ges 13: 222–334 (in German).

Pasquaré G (1968). Geology of the Cenozoic volcanic area of Central Anatolia. Rome, Italy: Atti della Accademia nazionale dei Lincei.

Pasquaré G, Poli S, Vezzoli L, Zanchi A (1988). Continental arc volcanism and tectonic setting in Central Anatolia, Turkey. Tectonophysics 146: 217–230.

Retallack GJ (1990). Soils of the Past: An Introduction to Palaeopedology. London, UK: Unwin Hyman.

Rollinson HR (1993). Using Geochemical Data: Evaluation, Presentation, Interpretation. New York, NY, USA: John Wiley and Sons.

Sánchez C, Galán E (1995). An approach to the genesis of palygorskite in a Neogene-Quaternary continental basin using principal factor analysis. Clay Miner 30: 225–238.

Sancho C, Melendez A, Signes M, Bastida J (1992). Chemical and mineralogical characteristics of Pleistocene caliche deposits from the central Ebro Basin, NE Spain. Clay Miner 27: 93–308.

Schumacher R, Keller J, Bayhan H (1990). Depositional characteristics of ignimbrites in Cappadocia, Central Anatolia, Turkey. In: Savaşcın MY, Eronat AH, editors. Proceedings of the International Earth Science Congress on Aegean Regions (IESCA-1990), Vol. 2. pp. 435–449.

Schumacher R, Mues-Schumacher U (1996). The Kızılkaya ignimbrite-an unusual low-aspect-ratio ignimbrite from Cappadocia, central Turkey. J Volcanol Geoth Res 70: 107–121.

Schumacher R, Schumacher UM (1997). The pre-ignimbrite (phreato) plinian and pheratomagmatic phases of the Akdag-Zelve ignimbrite eruption in Central Anatolia, Turkey. J Volcanol Geoth Res 78: 139–153.

Şengör AMC, Yılmaz Y (1983). Türkiye'de Tetis'in evrimi: Levha tektoniği açısından bir yaklaşım. Ankara, Turkey: Türkiye Jeoloji Kurumu Yerbilimleri Özel Dizisi (in Turkish).

Soil Survey Staff (1998). Keys to Soil Taxonomy. 8th ed. Washington, DC, USA: US Department of Agriculture, Natural Resources Conservation Service.

Suárez M, Robert M, Elsass F, Martin Pozas JM (1994). Evidence of a precursor in the neoformation of palygorskite- new data by analytical electron microscopy. Clay Miner 29: 255–264.

Talbot MR (1990). A review of the paleohydrological interpretation of carbon and oxygen isotopic-ratios in primary lacustrine carbonates. Chem Geo 80: 261–279.

Talbot MR, Kelts K (1990). Paleolimnological signatures from carbon and oxygen isotopic ratios in carbonates from organic carbon-rich lacustrine sediments. In: Katz BJ, editor. Lacustrine Basin Exploration: Case Studies and Modern Analogs. Tulsa, OK, USA: American Association of Petroleum Geologists, pp. 88–112.

Taylor SR, McLennan SM (1985). The Continental Crust: Its Composition and Evolution. Oxford, UK, Blackwell.

Temel A (1992). Kapadokya eksplozif volkanizmasının petrolojik ve jeokimyasal Özellikleri. PhD, Hacettepe University, Ankara, Turkey (in Turkish).

Temel A, Gündoğdu MN, Gourgaud A, Le Pennec JL (1998). Ignimbrites of Cappadocia (Central Anatolia, Turkey): petrology and geochemistry. J Volcanol Geoth Res 85: 447–471.

Toprak V (1996). The origin of the Quaternary basins which have been developed in the Cappadocia volcanic subsidence, Central Anatolia. Trabzon, Turkey: 30th Year Symposium, Karadeniz Technical University, pp. 326–340.

Toprak V (1998). Vent distribution and its relation to regional tectonics, Cappadocian Volcanics, Turkey. J Volcanol Geoth Res 85: 55–67.

Valero Garcés BL, Gierlowski-Kordesch EH, Bragonier WA (1997). Pennsylvanian continental cyclothem development: no evidence of direct climate control in the Upper Freeport Formation (Alleghenian) of Pennsylvania. Sediment Geol 109: 305–320.

Verrecchia EP, Le Coustumer MN (1996). Occurrence and genesis of palygorskite and associated clay minerals in a Pleistocene calcrete complex, Sde Bowuer, Negev Desert, Israel. Clay Miner 31: 183-202.

Viereck-Goette L, Lepetit P, Gürel A, Ganskow G, Çopuroğlu İ, Abratis M (2010). Revised volcanostratigraphy of the Upper Miocene to Lower Pliocene Ürgüp Formation, Central Anatolian volcanic province, Turkey. GSA Special Papers 464: 85–112.

Wright VP, Platt NH (1995). Seasonal wetland carbonate sequence and dynamic catenas: a re-appraisal of palustrine limestones. Sediment Geol 99: 65–71.

Wright VP, Tucker ME (1991). Calcretes. Oxford, UK: Blackwell.

Xu Q, Ding L, Zhang L, Cai F, Lai Q, Yang D, Liu-Zeng J (2013). Paleogene high elevations in the Qiangtang Terrance, central Tibetan Plateau. Earth Planet Sci Lett 362: 31–42.

Yalçın H, Bozkaya O (2011). Sepiolite-palygorskite occurrences in Turkey. In: Galán E, Singer E, editors. Developments in Palygorskite-Sepiolite Research. A New Outlook on these Nanomaterials. Developments in Clay Science, Vol. 3. Amsterdam, the Netherlands: Elsevier, pp. 175–200.

Yavuz-Işık N, Toprak V (2010). Palynostratigraphy and vegetation characteristics of Neogene continental deposits interbedded with the Cappadocia ignimbrites (Central Anatolia, Turkey). Int J Earth Sci (Geol Rundsch) 98: 949–1184.

Yıldız FE, Dilaver AT, Gürer İ, Ünsal N, Bayari S, Türkileri S, Çelenk S (2008). Develi kapalı havzası'nda yeraltı suyu ve yüzey suyu ilişkisinin doğal izotoplarla belirlenmesi. İstanbul, Turkey: Devlet Su İşleri Genel Müdürlüğü, III. Hidrojeolojide İzotop Teknikleri Sempozyumu, pp. 20–35.